Master of Engineering

Design of efficient transition metal-based electrocatalyst for hydrogen evolution reaction

The Graduate School
of the University of Ulsan

Department of Civil and Environmental Engineering
Yasamin Shajirati

Design of efficient transition metal-based electrocatalyst for hydrogen evolution reaction

Supervisor : Professor Lee, Byong-Kyu

A thesis

Submitted to

The Graduate School of the University of Ulsan in partial Fulfillment of the Requirements for the Degree of

Master of Environmental Engineering

by

Yasamin Shajirati

Department of Civil and Environmental Engineering

University of Ulsan, Korea

Dec. 2023

Design of efficient transition metal-based electrocatalyst for hydrogen evolution reaction application

This certified that the master thesis of

Yasamin Shajirati is approved

Committee Chairman: ……

Prof. Seok-Young Oh

Committee Member: ……

Prof. Daeseung Kyung

Committee Member: ……

Prof. Byeong-Kyu Lee

Department of Civil and Environmental Engineering

University of Ulsan, Korea

Dec. 2023

ACKOWLEDGMENT

I would like to appreciate my professor's support, kindness, and consideration. I was lucky to be tutored throughout by prof. Byeong-Kyu Lee. I would like to thank my committee members including prof. Seok-Young Oh, Prof. Daeseung Kyung, and Prof. Byeong-Kyu Lee for taking time out of their busy schedule to serve in my committee, review my thesis and provide valuable comments and suggestions on my work. Along with this, I would like to thank other professors in the department of Civil & Environmental Engineering for their help and support during my Ms. courses. I would like to show my gratitude toward my family who always being my rock.

Finally, I wish to acknowledge the University of Ulsan for providing me with a full scholarship, without which this work could have never begun.

Ulsan, Dec. 2023

Yasamin Shajirati

Contents

Table of figures

List of Tables

List of Acronyms

TMs…Transition metals

HER…Hydrogen evolution reaction

EDS…Energy-dispersive X-ray spectroscopy

XRD… X-ray diffraction

NF…Nickel foam

LSV… Linear sweep voltammetry

EIS… Electrochemical impedance spectroscopy

AWE… Alkaline water electrolysis

PEMs… Proton exchange membranes

SOE… Solid oxide water electrolysis

OER… Oxygen evolution reaction

CMP… Cobalt Molybdenum Phosphate

TMCs… Transition metal carbides

TMSs…Transition metal sulfides

RHE… Reversible hydrogen electrode

SAE…Single atom electrocatalyst

LDH…Layered double hydroxide

SEM… Scanning electron microscope

TEM…Transmission electron microscope

XPS…X-ray photoelectron spectroscopy

CV… Cyclic voltammetry

CP… Chronopotentiometry

Cdl… Electrochemical double-layer capacitance

WE… Water electrolysis

AEMs… Alkaline anion exchange membranes

Eq…Equation

DFT… Density functional theory

TMPs…Transition metal phosphides

TMNs…Transition metal nitrides

ΔG_H ... Gibbs free energy of hydrogen adsorption

HRTEM…High-resolution transmission electron microscopy

Abstract

Electrochemistry is a foundation science addressing many environmental issues by shifting from fossil fuel to zero-carbon world. Many research groups are using electrochemistry principles to solve environmental challenges. To address these environmental and energy issues, a lot of efforts have been made using experimental and theoretical approaches. Among all the strategies, electrocatalytic water splitting is a chemically simple large-scale method and a convenient technique to generate clean H_2. The desired electrocatalysts should exhibit high catalytic activity, durability, and minimum overpotential. Up to now, most of the electrocatalysts have minimum overpotential utilizing Pt/C photoanode, which is expensive to be used in practical markets.

Transition metals (TMs) have attracted great interest from researchers because they have great thermal stability and many lone-pair electrons with unique electron orbital structures. Their sufficient number of lone pair electrons make them a good candidate for improving their intrinsic catalytic activity by shifting the d-band center.

Unfortunately, their reported catalytic performance as TMs electrocatalysts for green H_2 production can hardly be comparable to those of commercial catalysts. Until now, a lot of modifications have been studied, such as defect engineering, metal or non-metal doping, heterostructure and interface engineering, to improve their catalytic activities for hydrogen evolution reaction (HER).

In this thesis, both metal doping and adding LDH as co-catalyst have been adopted to modify performance of fabricated electrode.

Thesis Outline

The purpose of this thesis is the design of stable, low-cost, and efficient electrocatalyst to boost hydrogen evolution reaction.

The thesis is organized as follow; chapter 1 (introduction) includes the objective of this research study, the background of the very recent progress, and strategies for improving the performance of electrocatalyst and especially decreasing overpotential required for HER. In chapter 2, materials and synthesis method have been explained. In the third chapter, the morphological investigation of the CoMoP and other prepared electrodes was characterized by a scanning electron microscope (SEM), energy-dispersive X-ray spectroscopy (EDS) and a transmission electron microscope (TEM). The structural and crystallinity properties of the prepared thin films were investigated through X-ray diffraction (XRD). X-ray photoelectron spectroscopy analyzed the chemical components and consisted of elements. Electrochemical performance was measured using CV, EIS, LSV and Tafel test. The stability of electrocatalysts was examined by chronopotentiometry (CP) and by using a graphitic electrode as the counter electrode. Finally, chapter 4 contains the conclusion. Finally, Chapter 5 explains about future work.

Chapter 1: Introduction

1.1. Climate change and Electrochemistry

Climate change has been defined as a steady change of the weather average pattern. The reason of climate change can be naturally or artificially[1]. In the past two centuries, human activities are the main cause of shift in temperature and weather pattern [2]. Burning fossil fuels for generation electricity is one of the main causes of climate change. Methane, carbon dioxide, and nitrous oxide are three known major of greenhouse gas[1]. Paris Climate Agreement in 2015 obligated 197 countries to mitigate climate change until 2030 and limit global warming to levels well below 2 ◦C relative to pre-industrial levels[3]. In support of this agreement, energy and greenhouse reduction has been a national goal of south Korea[4]. Bases on the report of the greenhouse gas inventory and research center of south Korea, national greenhouse gas emissions in 2020 were 656.22 million tons, decreased 6.4% compared to the previous year. (See Fig.1-1) Korea energy policies seek to enhance the proportion of renewable electricity generation along with reduction of thermal and nuclear power generation[3].

Fig. 1-1 demonstrates emission trajectory up to 2050 carbon neutrality, emission target at nationally determined contributions (NDC), and historical GHG emissions. several policies have been implemented to achieve this goal, the government suggested some measures that consist of expanding renewable energy generation reducing oil, and coal power generation[3].

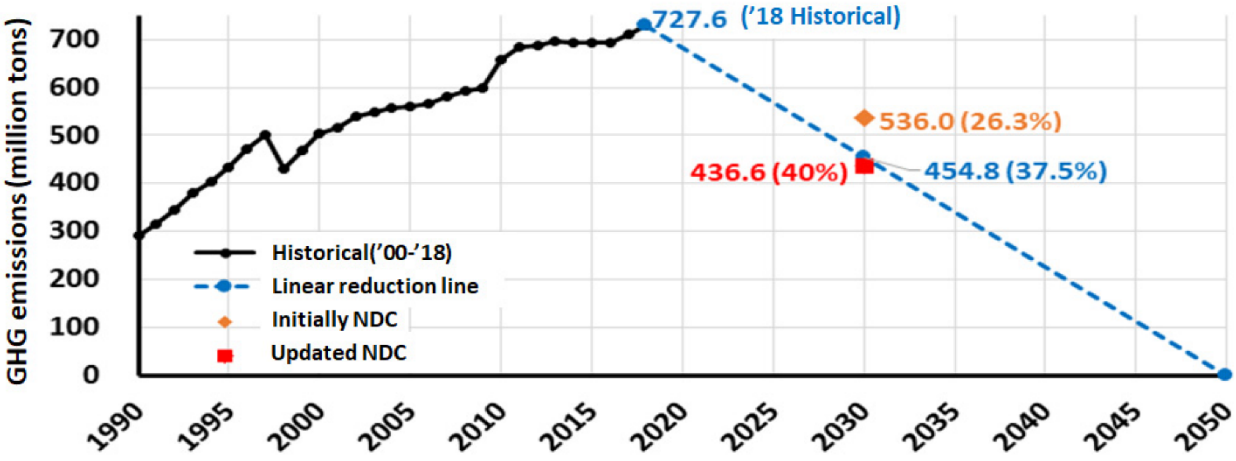

Fig. 1-1 Historical GHG emissions, emission target of Korea, and 2050 net-zero [3]

With that in mind, using more environmental-friendly methods for producing electricity is essential. There is an urgent need for transition toward clean and sustainable energy sources to reach carbon neutrality goal. To reach this goal, significant research have been done to replace

fossil fuel energy in order to reduce the energy sector's carbon footprint[5]. Geothermal, hydroelectric, solar energy, and nuclear are clean alternatives while despite all their merits, their demerits overshadow their merits. For instance, waste disposal challenges of nuclear fission energy and difference solar energy illumination in different area and time of day and less predictable generation of common renewable energy sources, all suggest finding alternative clean, safe, accessible, and sustainable energy source as an alternative. Along with this, power storage is another challenge to enhance energy efficiency reliability, control, and energy quality[6].

Hydrogen is an alternative energy carrier, which is estimated to play an important role in future energy [7]. Eco-friendly production process and ability to produce electricity without any toxic emissions are appealing feature of H_2 for industrial-scale usage[6].

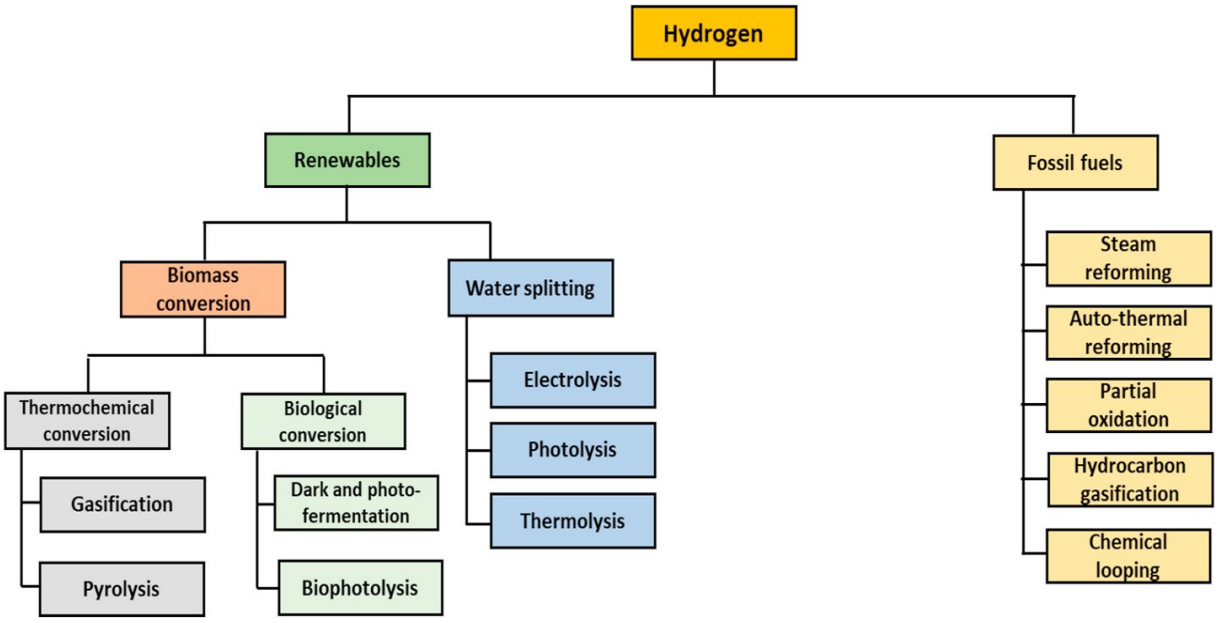

Fig. 1-2 Notable technologies for hydrogen production [7].

1.2. Hydrogen production technologies

There are many pathways for producing hydrogen, based on the energy resource categorized on two group of fossil fuels and renewable energy (Fig 1-2)[7]. Several technologies based on

different pathways, feedstocks, and renewable or non-renewable sources are mentioned in Fig.1-2. Numerous materials naturally can be hydrogen sources for instance water[8] or biomass. As it obvious in Fig.1-3, finding environmental-friendly method along with high energy yield is quite a challenge.

For instance, steam methane reforming (SMR) produce about 80% of hydrogen production share in the world while also it is pioneer in producing Co_2 by using non-renewable feedstocks[6] .

Todays, cost effectiveness of natural gas make it popoular method for hydrogen production[8]. Unforunately, it is not environmental-friendly method, linked to various greenhouse emissions[8]. Among all aforesaid starategies, elctrocatalysis with net zero emission considered as sustainable way to produce green hydrogen.

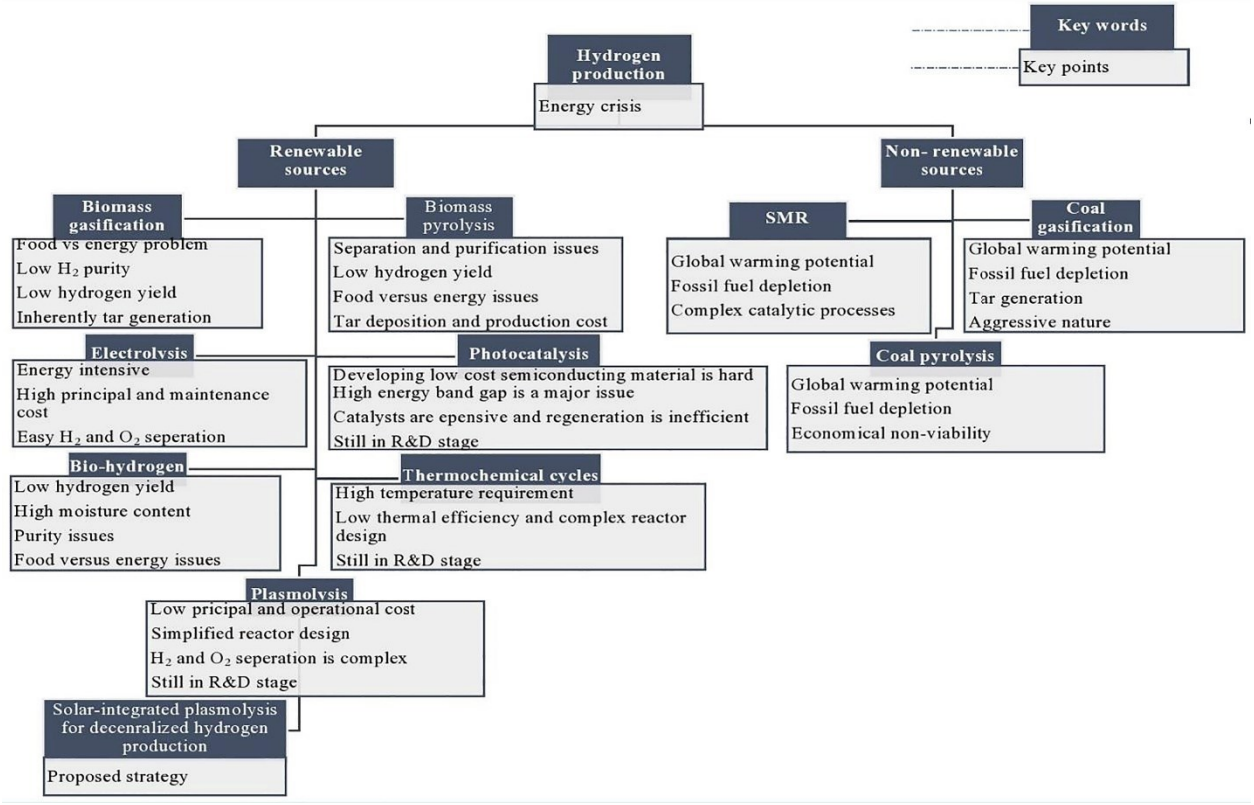

Fig. 1-3 Schematic representation of hydrogen production pathways [6].

1.3. Water electrocatalysis for hydrogen production technologies

Water splitting is electrochemical technique that use water as reactant and basic reaction is as fallow[9]:

$$\text{Anode: } H_20 \rightarrow 1/2\ O_2 + 2H+ + 2e^- \quad \text{Eq.1}$$

$$\text{Cathode: } 2H^+ + 2\ e^- \rightarrow H_2 \quad \text{Eq.2}$$

$$\text{Overall : } H_20 + \text{Electricity (237.2 kJ mol}^{-1}) + \text{Heat (48.6 kJ mol}^{-1}) \rightarrow H_2 + 1/2\ O_2 \quad \text{Eq.3}$$

As displayed in Fig.1-4, intermittent electricity produce by renewable sources and furthur excees electricity will use by water electrolysis system to produce green hydrogen[10]. Water electrolysis based on the elctrolyte used in electrolyzer have been categorized to alkaline water electrolysis (AWE), proton exchange membranes (PEMs), alkaline anion exchange membranes (AEMs), and solid oxide water electrolysis (SOE). Although the operating principles are the same for all mentioned electrolyte systems, operating condition and materials are different. Along with this, there are challenges must be addressed to use each of them in industrial scales. For instance, use precious metals in PEM electrolysis [9], limited stability of AEMs water electrolysis[11] and duarability of SOE[9]. Therefore, considerable developments are needed to overcome mentioned problems. On the contrary, AWE technology showed better electrochemical performance with higher duarability in comparsion with other technologies.

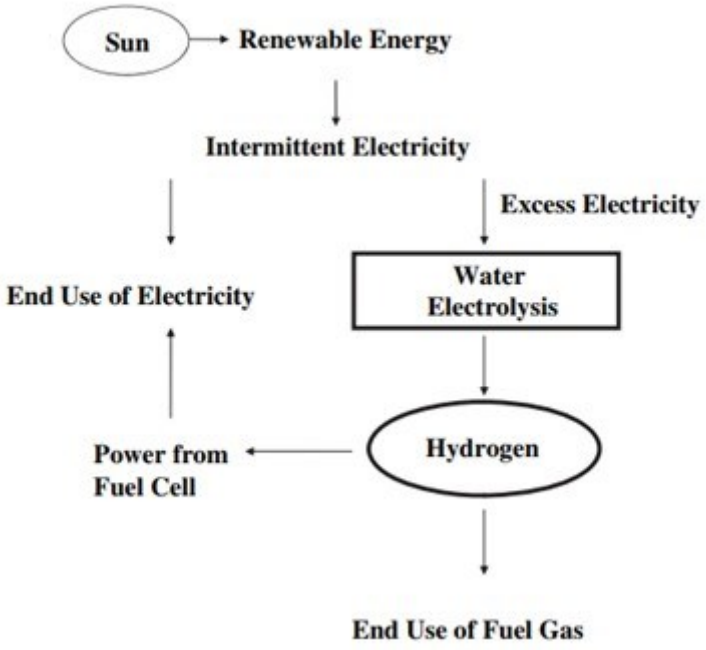

Fig. 1-4 A schematic of water electrolysis role in energy distribution system[12]

Along with this, it can be used more widely[11] and on the basis of different operating temperatures, low and high temperature water electrolysis are also possible[9]. Unfortunately, widespread commercial applications of AWE technology are restricted due to the cost too. So, developing non-noble metal based electrocatalyst is urgent.

1.4. Alkaline water electrolysis

Alkaline water electrolysis is the mature technology which has been used for using H_2 and O_2 since 1800 [12]. Since then,significant advancements have been achieved to whole water electrolysis system (see Fig.1-5), such as collection of gas bubble management and electrolyte improvement[12].

AWE is a multiphysics process which used electrical energy to split water into gasous H_2 and O_2. OER occures at the aonde while HER at cathode.In the other word, electrical energy converted to chemical enrgy at the electrodes, follow by storing as hydrogen energy[14]. The ideal electrode must show high efficiency, optimum structural features and long-term stability for HER. With that in mind , electrode engineering required to generate preparative quantity of H_2 with cost-effective materials[15].Recently, TMs or d-block gained extensive interest as a efficient and non-precious metal electrocatalysts.

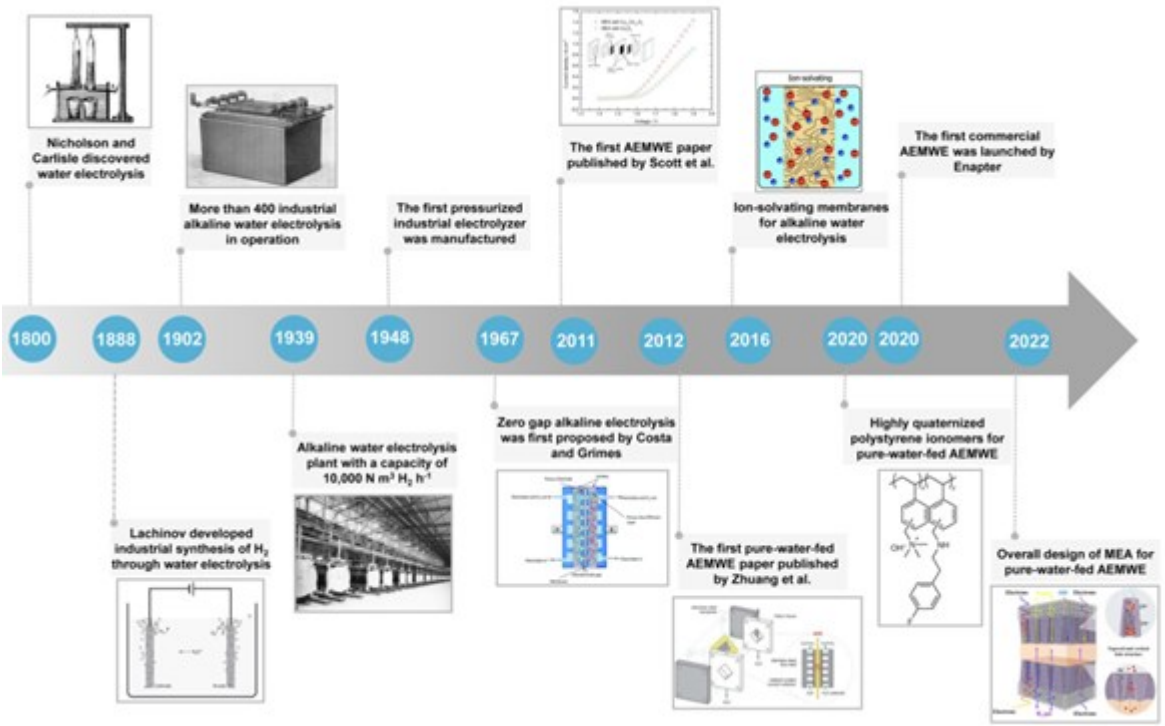

Fig. 1-5 Timeline of developments of AWE[10]

1.5. Transition metals

Transition metal or d-block elements have been extensively studied as electrocatalyst for HER due to their tunable physical and chemical properties[16]. Recent research advances indicate that combination of TMs with non-oxygen elements such as P, C, N_2, and S produce TMPs[17], TMCs[16], TMNs[18], and TMSs[19] could act as next generation of HER electrocatalyst (see Fig. 1-6). Transition metal phosphides (TMPs) are considered as capable electrocatalytic materials for HER as they possess unique physicochemical properties such as high electronic conductivity, durability, and high electrocatalytic activity for HER[20]. A theoretical and experimental study disclosed that TMPs have a trigonal prism structure due to the large atomic radius of P atom which significantly hinders the electron delocalization of the metals and increase intrinsic catalytic activity[21]. Likewise, multiple strategies have been used to modify electrocatalytic properties of TMPs toward HER, including hybridization and alloying of TMPs with highly conductive supports such as NF[22].

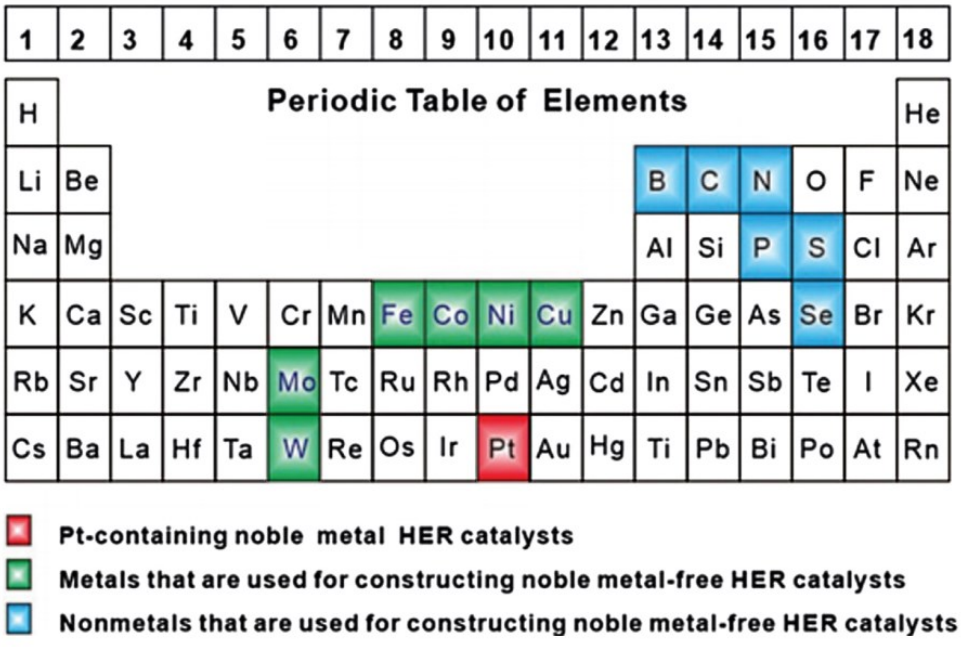

Fig. 1-6 Periodic table of the elements indicating the elements used in HER electrocatalysts [20].

1.6. Strategies to enhance electrochemical properties of TMs

Designing remarkable electrocatalysts with excellent HER performance is crucial. An excellent HER electrocatalyst must show long stability with minimum overpotential[22]. It is well ascertained that the increasing the number of active sites by strategy such as creating edge active sites, utilizing mesoporous structure, and downsizing the electrocatalysts will robust the catalytic activity[23]. Furthermore, the nature of an electrochemical reaction consists of absorption of reactants and intermediates on active site and product desorption[23]. In this regard, modulating electronic structure of catalyst followed by enhancing the intrinsic electroactivity of electrocatalysts by introducing impurity such as metal or non-metal or eliminating atom and creating vacancy in electrocatalyst structure will tune absorption properties[23]. Generally, there are different synthesis methods for fabrication of multi metallic TMPs electrocatalyst[24]. Zhang et al. used a gas-solid reaction approach for fabrication CoMoP nanosheets with good HER performance, which needs only 24 mV overpotential to reach a current density of 10 mA cm^{-2}[25]. Similarly, Ray and co-worker adapted gas-solid reaction approach for growth of bifunctional catalyst on carbon cloth, which required cell voltage of 1.54 V to reach the 10 mA cm^{-2} current density[26]. Shamloofard and Shahrokhian prepared star-like zinc–cobalt-sulfide decorated with cobalt–molybdenum-phosphide as a bifunctional electrocatalyst, via a combination of three-step hydrothermal–sulfidation–electrodeposition processes. In regard to HER performance, the prepared electrocatalyst required an overpotential of 202 mV to attain the current density of 200 mA cm^{-2}. Zhai and co-workers used carbonization and metal-organic frameworks approach for embedding cobalt phosphide nanoparticles in mesoporous nitrogen-doped graphitic carbon materials. This bifunctional electrocatalyst needed only 98 mV overpotential at 10 $mAcm^{-2}$[27].

Techniques such as heteroatom doping, vacancies, heterostructures, strain and phase transition could effectively regulate the electron configuration of neighboring atoms by causing tensile or compressive effects in the host materials[28]. For instance, Li and co-workers used molten salt synthesis strategy to fabricate defect-rich CoP/Co_2P electrocatalyst. The prepared electrode showed the bifunctional electrocatalytic behavior toward both HER and oxygen evolution reaction (OER). For achieving 10 $mAcm^{-2}$ current density, it needed 190 mV overpotential[29]. Chang Et al. investigated HER performance of nanoplate arrays of S-Ni5P4 NPA/CP (sulfur-doped nickel phosphide on carbon paper). Sulfur doping showed a good effect on the HER performance, which needs 56 mV overpotential to achieve 10 $mAcm^{-2}$current density [30].

Along with this, Heterostructuring enabled using a catalyst that include components with different functionalities and efficiently catalyze the dissociation of water and consequently promote the HER in a neutral and a alkaline media. The construction of crystalline/amorphous interface engineering is another strategy to achieve fast mass diffusion and fast electron transfer during electrocatalysis. Yang et al. used phosphorization approach to construct nickel phosphide/ molybdenum dioxide/nickel foam heterostructure nanorods arrays (Ni_2P/MoO_2/NF HNRs) [17] .Their prepared electrode required overpotential of 34 mV at 10 $mA \cdot cm^{-2}$ current density. Chen et al. achieved interface-engineered crystalline/amorphous Co_2P/CoMoPx nanostructure by an electrodeposition method, which needed an overpotential of 121 mV at 100 $mA \cdot cm^{-2}$ [31].

Beside from synthesis route, material properties of TMPs are important in shaping particle and size distribution[20] . For instance, dual cations with unsaturated coordination and high electrical conductivity (Mn, Fe, Co, Ni, Cu, and V, etc.) can act as active catalytic centers in HER[16]. Therefore, appropriate combination of techniques togethers could increase the performance of electrocatalyst.

1.7. CoMoP

TMPs, particularly CoP catalysts, have attracted great interest from researchers because they have great thermal stability and unique electron orbital structures. Their sufficient number of lone pair electrons make them a good candidate for improving their intrinsic catalytic activity by shifting the d-band center [32,33]. Up to date, several transition metal phosphides, such as CoMoP [25,34,35], P-CoMoS [26], NiCoP [36] and MoOxSy-CoPI [37] have been fabricated [24]. Unfortunately, their reported catalytic performance as CoP catalysts for green H_2 production can hardly be comparable to those of commercial catalysts. Therefore, a lot of modifications studied, such as defect engineering, metal or non-metal doping, thickness tuning, heterostructure and interface engineering, to improve their catalytic activities for HER [24,38]. Dual doping is regarded as one of the promising approaches for enhancing active sites and intrinsic activity of electrocatalysts.

Theoretical and experimental studies showed embedding transition metal dopant into Co structure would optimize the absorption of Gibbs free energy of the intermediates and regulate their electronic state [32,39]. For example, the CMP appears to have excellent HER activity as

it has the advantage of a lower ΔG_H value of - 0.555 eV, calculated based on the density functional theory (DFT). There have been many literatures about CMP synthesis methods and their different applications [25,38–42].

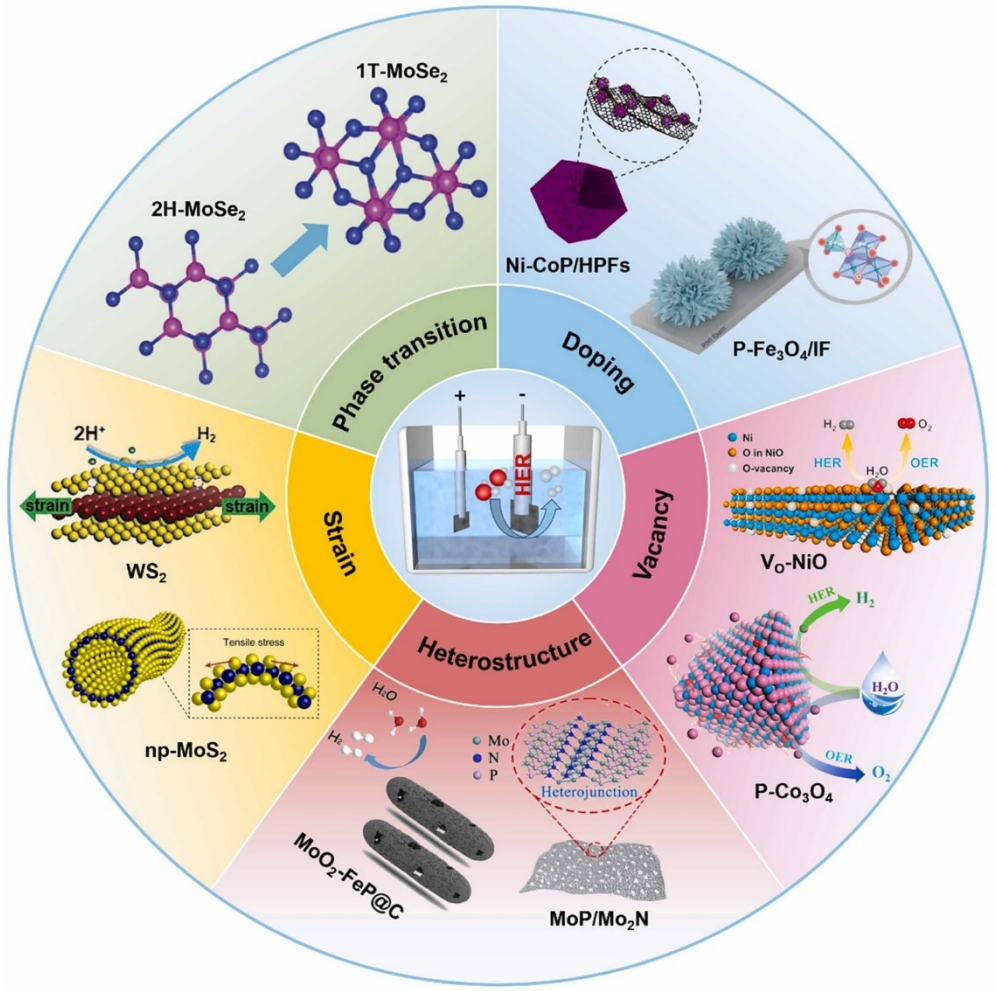

Fig. 1-7 Schematical illustration of electronic structure modulation of HER electrocatalysts [28].

1.8. Layered double hydroxides

Layered double hydroxides (LDHs) are a class of anionic clays consisting of positively charged layers with charge balancing anions between the layers[43]. Most LDHs may be represented by the generic formula $[M_{1-x}^{2+}\ M_x^{3+}(OH)_2]\ \ (A^{n-})_{x/n}.zH_2O$, where $A^{n-}$is a interlayer anion, x is stoichiometric coefficient and M^{2+} and M^{3+} are the divalent and trivalent metal ions located in the host layers [44]. Given their inherent positive charge and rich ionic surface –OH group, combination of LDH nanosheets or nanoparticles with other nanomaterials, generating

nanocomposites with promising nonprecious HER electrocatalysts in alkaline electrolyte solutions [45]. In particular, recent studied showed that CoFe-based LDHs is a promising HER electrocatalyst[46]. Given its sluggish water dissociation process and low electrical conductivity, several strategies have been adopted to improve its performance[46]. Construction of hierarchical architecture is a promising solution to enlarge surface area, facilitate the charge transfer and provide more active sites, therefore further accelerating the HER[47]. This study comparison the performance of CoNi, NiFe, and CoFe-LDH electrodeposition on the HER performance of CMP electrodeposited on the NF.

Chapter 2: Materials and Methods

2.1. Materials

2.1.1. Chemicals

Nickel (II) nitrate hexahydrate (Ni $(NO_3)_2 \cdot 6H_2O$), Potassium hydroxide (KOH), Iron (II) sulfate heptahydrate ($FeSO_4.7H_2O$), sodium molybdate (VI) dihydrate ($Na_2MoO_4.2H_2O$) were all received from Daejung Chemical & Metal Co., Ltd (Korea). Sodium citrate dihydrate ($Na_3C_6H_5O_7 \cdot 2H_2O$), sodium hypophosphite ($NaPO_2H_2$), Nafion (containing solution 5 wt%), Cobalt (II) nitrate hexahydrate ($Co(NO_3)_2 \cdot 6H_2O$) and commercial Pt/C product (10 wt%) were purchased from Sigma-Aldrich. Ethanol (99.9 wt%), Hydrochloric acid (HCl, 35-37%), and Acetone (99.9 wt%) were obtained from Samchun Co. (Korea). All the chemicals, reagents, and materials used in this study are of analytical grades and used as received without further purification unless otherwise stated. All aqueous solutions were prepared with deionized water in this study.

2.2. Methods

2.2.1. Electrodeposition of transition metal phosphides

CoP, MoP and CoMoP/NF were built on the NF surface through one-step procedure modified from Hao's work [39]. The CMP was electrodeposited on Ni foam substrates using a three-electrode electrochemical system which was immersed in an aqueous solution containing 0.44 g $Co(NO_3)_2.6H_2O$, 0.6 g $Na_3C_6H_5O_7.2H_2O$, 1.1 g $Na_2MoO_4.2H_2O$ and 2 g $NaPO_2H_2.H_2O$. For fabrication CoP, 1.8 g $Co(NO_3)_2.6H_2O$, 0.6 g $Na_3C_6H_5O_7.2H_2O$, and 2 g $NaPO_2H_2.H_2O$ have been dissolved in 100 ml deionized water and CoP electrodeposited on the nickel foam. In the case of MoP electrodeposition, 1.45 g $Na_2MoO_4.2H_2O$, 0.6 g $Na_3C_6H_5O_7.2H_2O$, and 2 g $NaPO_2H_2.H_2O$ same as CoP were all together dissolved in 100 ml deionized water and electrodeposited on the nickel foam. Electrodeposition potential of -1.0 V (vs. Ag/AgCl) for 60 s has been applied on all electrodes. Finally, the achieved electrodes were cleaned with purified water and then dried in an oven at 60 °C.

2.2.2. Electrodeposition of A-LDH (A= CoNi, NiFe, and CoFe-LDH) on CMP/NF

An aqueous solution of Ni $(NO_3)_2 \cdot 6H_2O$ (0.15 M) and $Co(NO_3)_2.6H_2O$ (0.15 M) was used as an electrolyte. Typically, a constant potential of -1.0 V vs Ag/AgCl for 50 s was applied to perform the deposition of CoNi-LDH on CMP. After washing the electrode with deionized water and drying it in an oven (60 ^{0}C) for an hour, CoNi-LDH/CMP/NF electrodes were prepared. Similarly, CoFe-LDH and CoNi-LDH are electrodeposited on CMP (See Fig.2-1). For investigating the doping influence of Mo, A-LDH has been electrodeposited on NF individually same as this procedure. For comparing HER performance of prepared electrodes with Pt/C, Pt/C ink was prepared by mixing 500 µL of ethanol, 4 mg of Pt/C powder, 485µL of deionized water, and 15µL Nafion (5.0 wt %), ultrasonically disperse to form a homogeneous catalyst ink. Then a portion of the solution (22.3µL) was dropped onto the 1 × 1 cm^2 Nickel Foam.

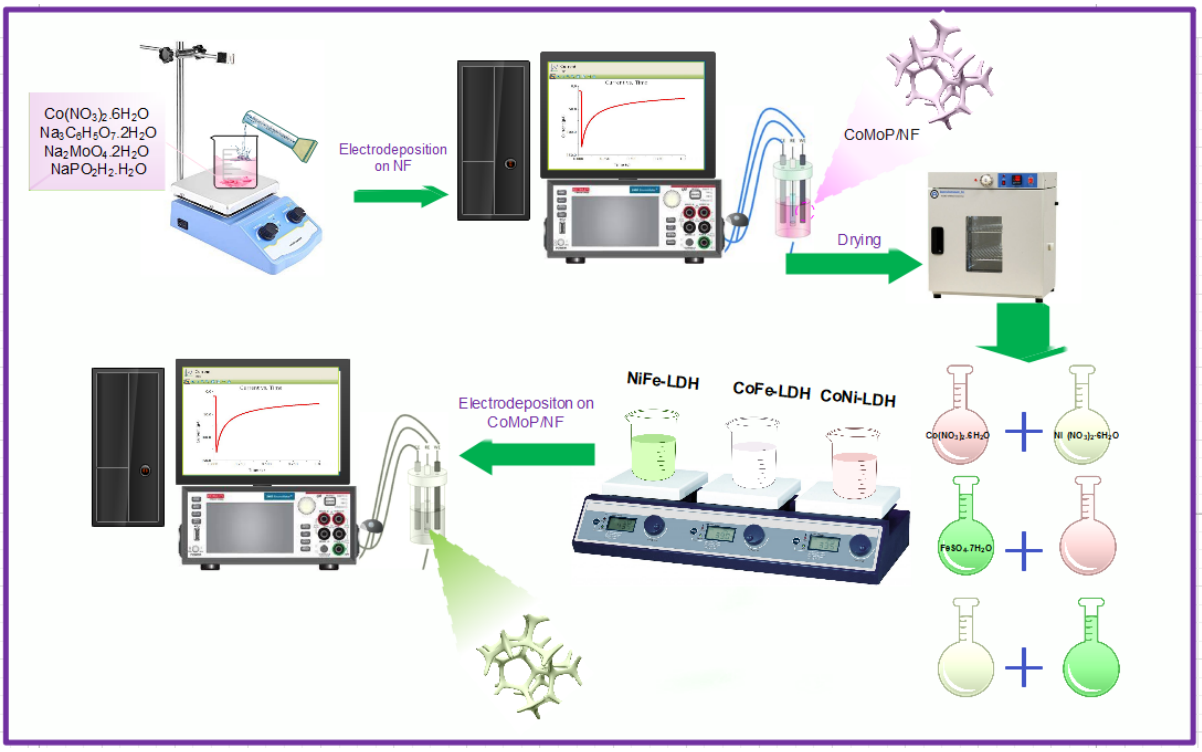

Fig. 2-1.Schematic illustrations of the fabrication process for porous A-LDH/ CoMoP/NF.

2.2.3. Characterization

XPS was used to investigate the surface electron states of the fabricated catalysts with ESCALAB 250XI. XRD was recorded on a high-power x-ray diffractometer D/MAX2500V/PC to analyze the crystal properties of materials in the 2θ range of 10^0-80^0. The microstructure of catalyst samples was observed by EDS and SEM and HR-TEM
(See table 2-1).

2.2.4. Electrochemical measurements

A potentiostat (VersaSTAT3, Princeton Applied Research) integrated with a 1.0 M Potassium hydroxide solution was used to measure HER activities of all the as prepared electrocatalysts at room temperature. The self-supported electrode (1 *1 cm), Pt wire, and Ag/AgCl electrode were used as the working electrode, counter electrode, and reference electrode, respectively. In this study, the equation shown in equation (1) has been used for converting the potential value to a reversible hydrogen electrode (RHE):

$$E_{RHE} = V_{Ag/AgCl} + 0.197 + 0.059 \times pH \quad \text{Eq. (1)}$$

CV at a potential region ranging from 0.941 to 1.04 V (vs. RHE) has been used to assess the C_{dl} under different scan rates (5, 10, 20, 30, 40, 50, 60 and 100 mV s^{-1}). The LSV is carried out at two different scan rates (5,10 mV s^{-1}). The stability of electrocatalysts was examined by chronopotentiometry (CP) in 25 mA cm^{-2} and by using a graphitic electrode as the counter electrode. The EIS was measured from 10^5 to 0.1 HZ.

Table 2-1. Characterization Details.

Characterization	Name	Device model	Purpose
Physical characterization	XPS (X-ray photoelectron spectroscopy)	ESCALAB 250XI	To investigate the surface electron states of electrodes
	XRD (X-ray photoelectron spectroscopy)	high-power X-ray diffractometer D/MAX2500V/PC	To analyze the crystal properties of materials
	SEM and EDS (scanning electron microscopy, energy-dispersive X-ray spectroscopy)	Nano230 FE-SEM	To observe microstructure of catalyst samples
	HR-TEM (High-resolution transmission electron microscope)	HRTEM, JEOL-2100 F	To observe microstructure of catalyst samples
Electrochemical characterization	CV (Cyclic voltammetry)	potentiostat (VersaSTAT3, Princeton Applied Research	To assess the electrochemical double-layer capacitance
	LSV (Linear sweep voltammetry)		To assess the performance
	CP(Chronopotentiometry)		Stability
	EIS (Electrochemical impedance spectroscopy)		To understand dynamic of the HER process, properties of electrode

Chapter 3: Results and Discussion

3.1. Physical characterization

The synthesis procedure can be observed in Fig.3-1. First, CMP was electrodeposited on a substrate (3D porous NF) followed by electrodeposition of A-LDH on CMP at constant time and potential. During the first electrodeposition, Co^{2+} and $Mo^{\delta+}$ cations were reduced while the negatively charged P atoms draw electrons from metal atoms [31] as displayed in equations (1) and (2):

$$MoO_4^{2-} + Co^{2+} + 8H^+ + 8e^- \rightarrow CoMo + 4\,H_2O \qquad \text{Eq. (1)}$$

$$CoMo + x(H_2PO_2^-) \rightarrow CoMoP_x + x\,OH^-. \qquad \text{Eq. (2)}$$

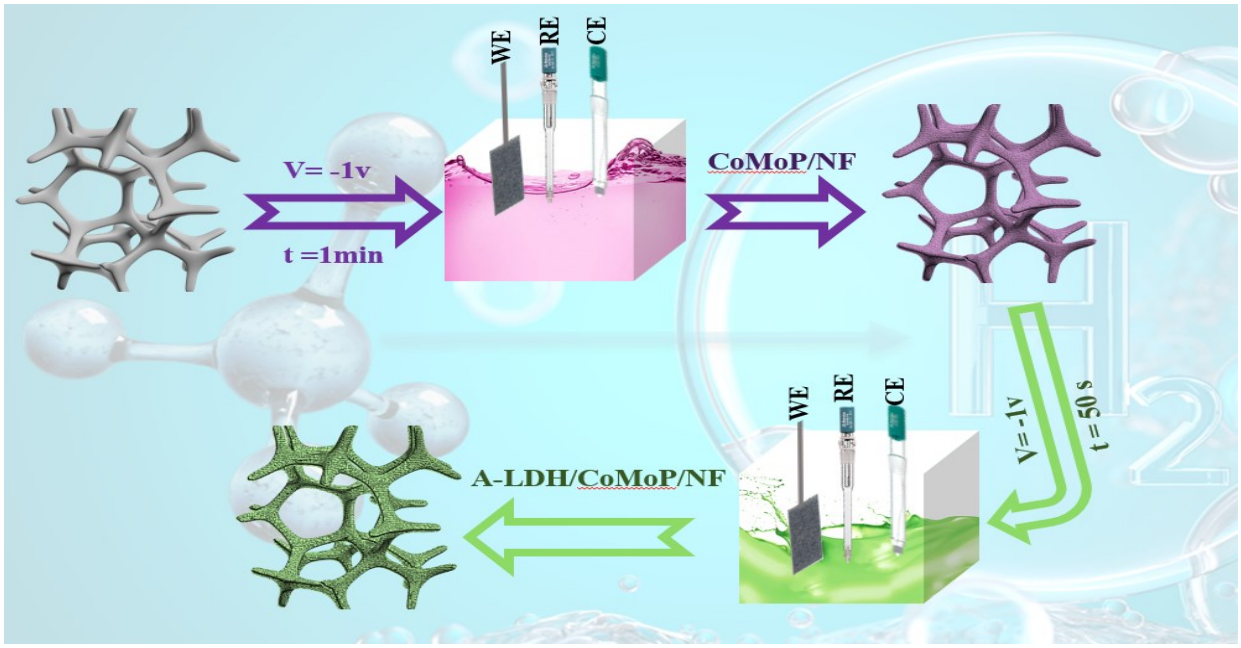

Fig. 3-1 Illustration of the preparation of the electrocatalyst

3.2. Materials morphology and structure

To find out how the composition affects the HER activity, SEM, HR-TEM, EDS mapping, XRD patterns, and XPS analyses of the as-prepared catalysts were conducted. Figs. 3-3b-c and Fig.3-2a-b show a uniform distribution of cobalt, molybdenum, and phosphorus on the surface of the electrode after electrodeposition of MoP, CoP and CMP on the nickel foam. To compare the structure of achieved electrocatalysts after electrodeposition, an image of bare nickel foam

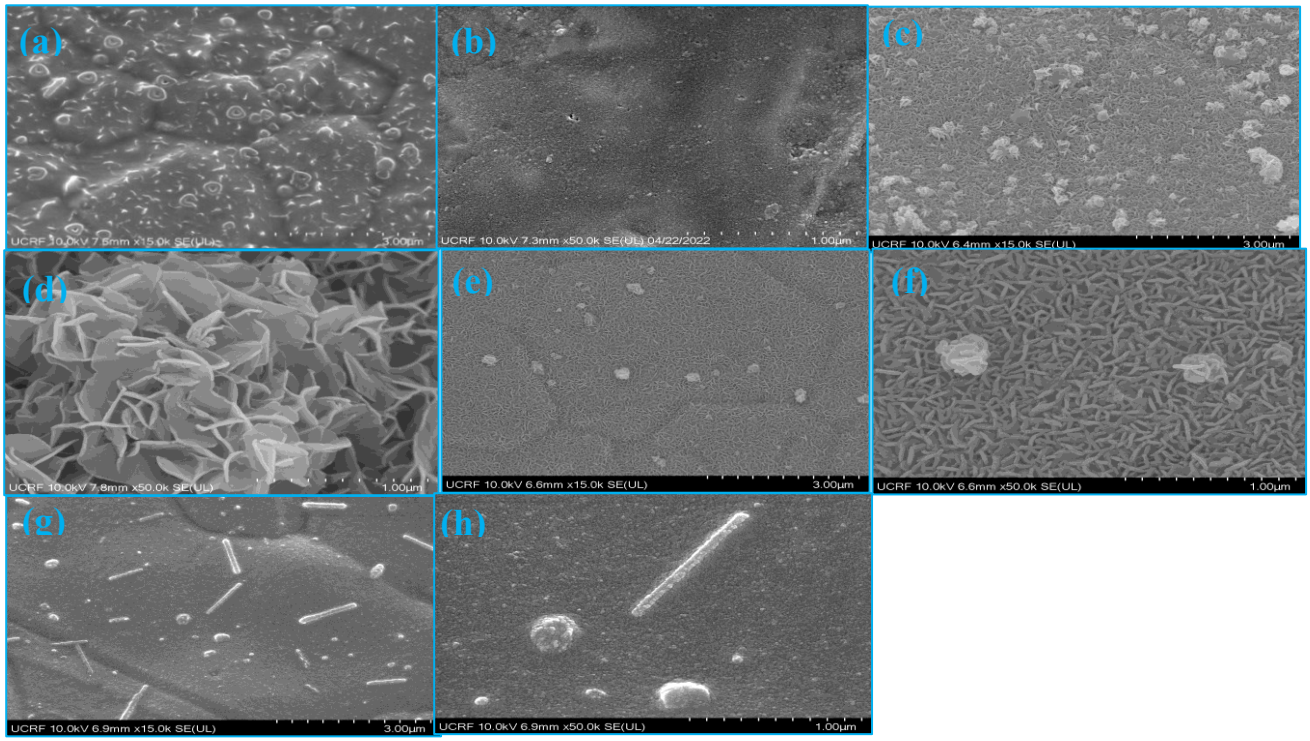

Fig. 3-2 SEM images of a-b) CMP, c-d) CoFe-LDH/CMP, e-f) NiFe-LDH/CMP, g-h) CoNi-LDH/CMP

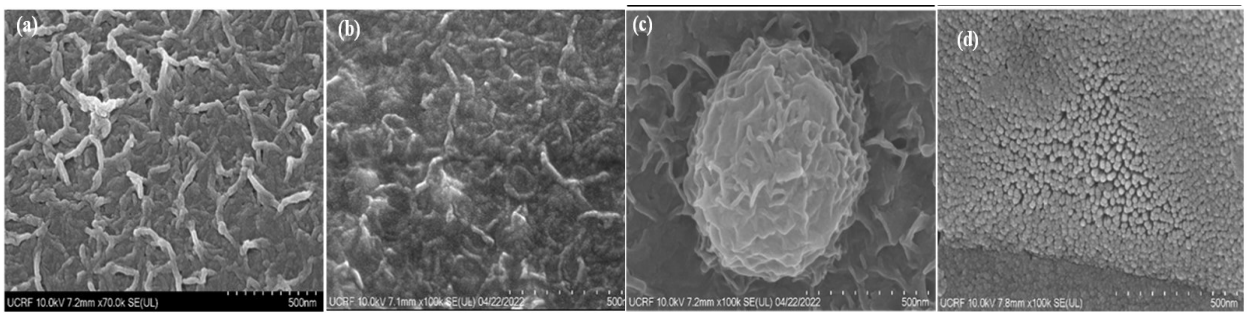

Fig. 3-3 .SEM images of a) NF bare, b) MoP/NF, c) CoP/NF, d) Pt/C

has been shown in Fig.3-3a. Also, the presence of homogeneously distributed small Pt nuclei has been illustrated in Fig. 3-3d. The surface morphology of the as-electrodeposited CoMoP was investigated using their SEM images (Fig.3-2a-b). After electrodeposition of A-LDH on the CMP, there was a significant change of resulting materials (Figs. 3-2c-h), in which the obtained CoFe-LDH and NiFe-LDH on the surface of CMP occurred under the form of flowers like structure which had interconnected with each other to generate a 3D network. On the other hand, CoNi-LDH electrodeposited on the CMP exhibits different structures (Fig. 3-2g-h). EDS results (see Figs. 3-4 to 3-7) further show the presence of Co, Mo, P, Ni, and Fe elements. Meanwhile, the blue color that belongs to Ni, overshows other colors in all EDS mapping

results, contributing to the superior composition of Nickel in all samples.

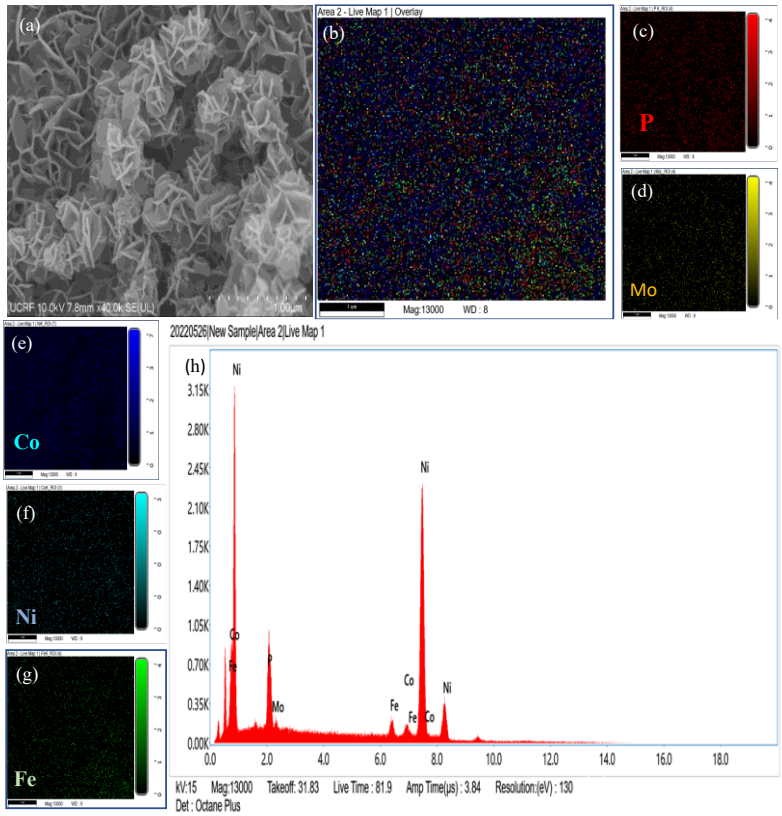

Fig. 3-4 SEM image CoFe-LDH/CoMoP/NF and EDS mixed color mapping of the b) CoFe-LDH/CoMoP/NF and color mapping of c) P, d) Mo, e) Ni, f) Co, g) Ni and EDS spectrum of h) CoFe-LDH/CoMoP/NF.

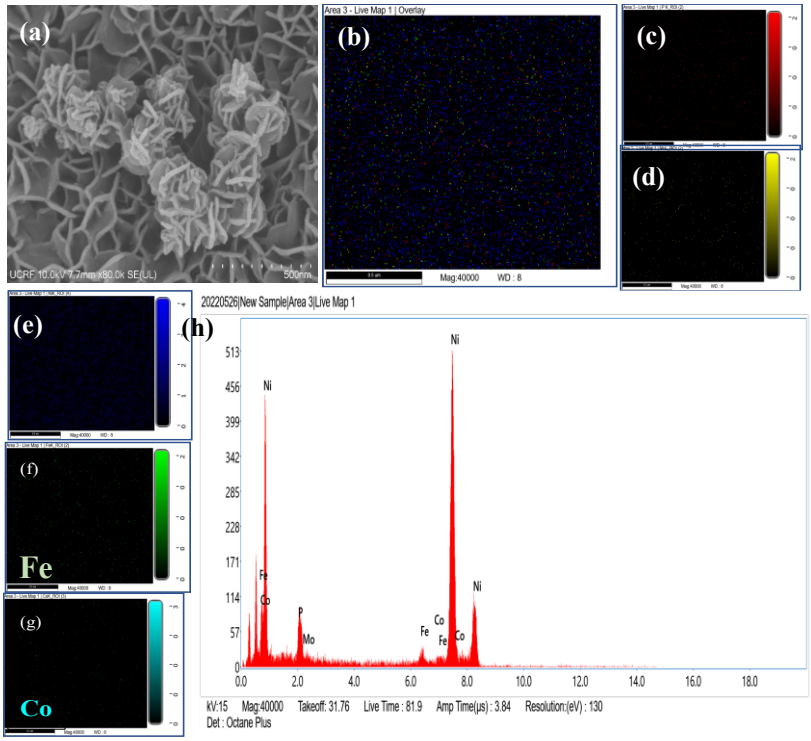

Fig. 3-5 a) SEM image of NiFe-LDH/CMP/NF and EDS mixed color mapping of the b) NiFe-LDH/CMP/NF and color mapping of c) P, d) Mo, e) Ni, f) Fe, g) Co and EDS spectrum of h) NiFe-LDH/CMP/NF.

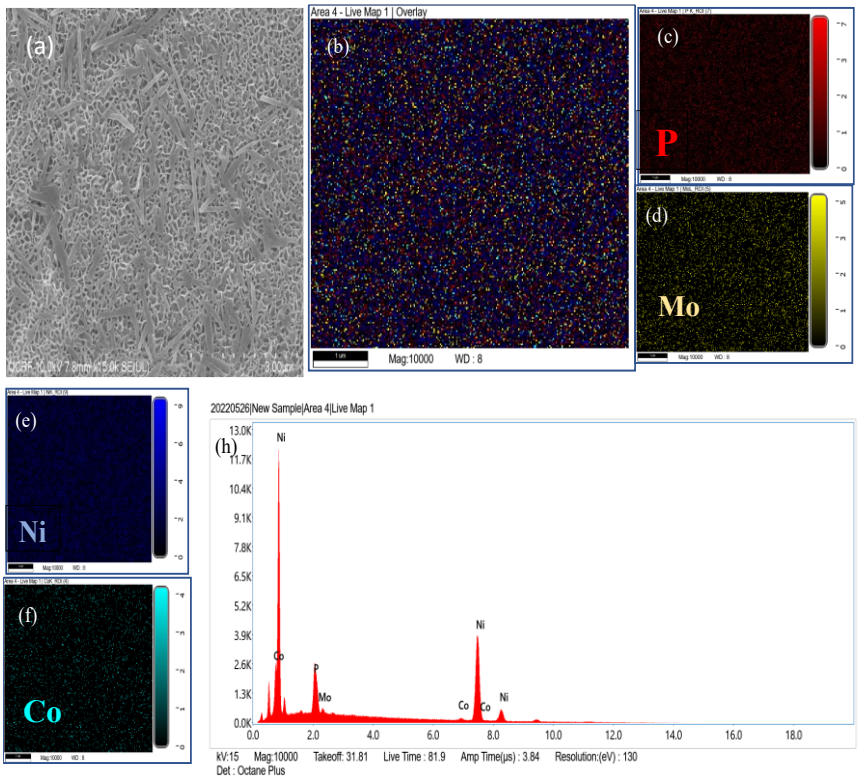

Fig. 3-6 a) SEM image of CoNi-LDH/CMP/NF and EDS mixed color mapping of the b) CoNi-LDH/CMP/NF and color mapping of c) P, d) Mo, e) Ni, f) Co and EDS spectrum of h) CoNi-LDH/CMP/NF.

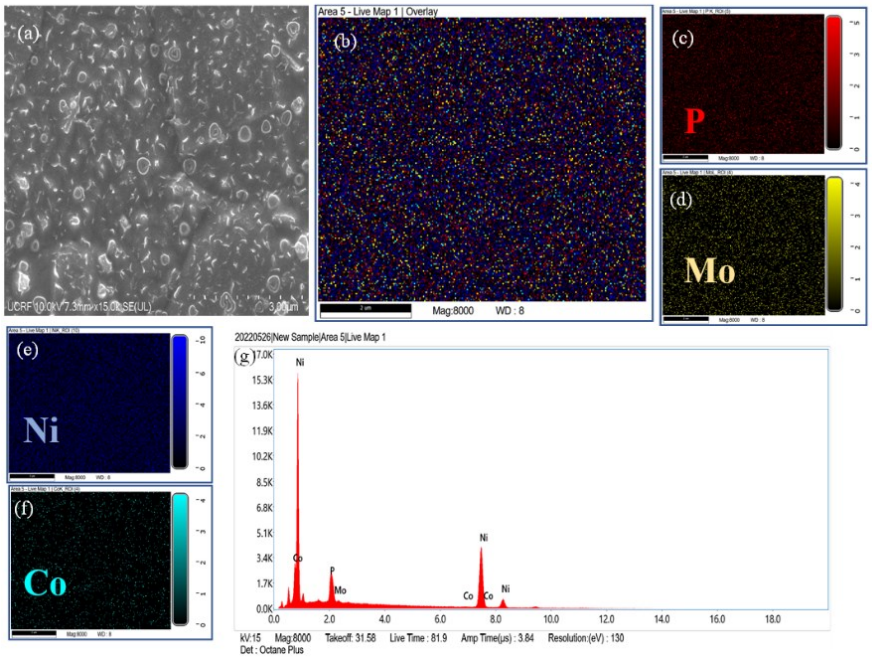

Fig. 3-7 . a) SEM image of CMP/NF and EDS mixed color mapping of the b) CMP/NF and color mapping of c) P, d) Mo, e) Ni, f) Co and EDS spectrum of g) CMP/NF.

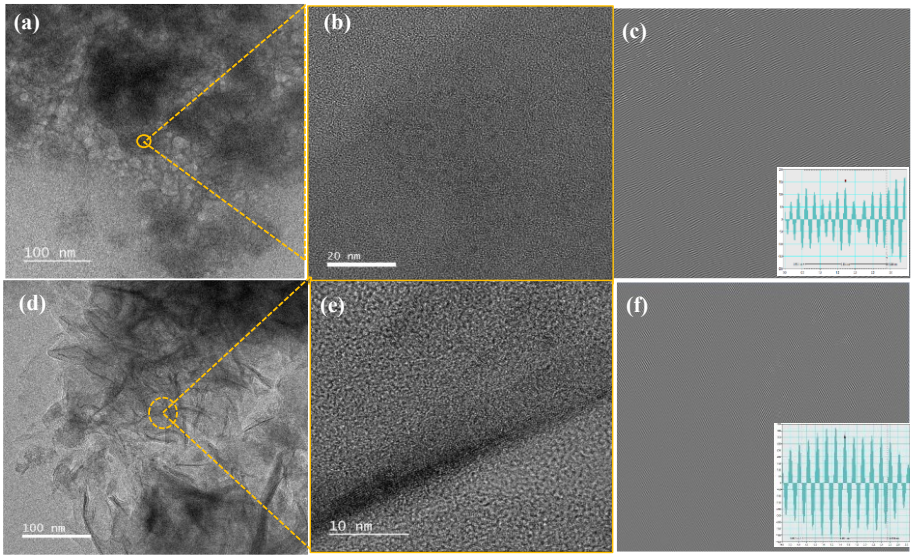

Fig. 3-8 HRTEM images of the a-b) CMP/NF and c) line profile and inverse FFT of CMP/NF image, d-e) CoFe-LDH/CMP/NF and f) line profile and inverse FFT of CMP/NF image.

High-resolution TEM images (Fig. 3-8) imply the poor crystallinity structure of CMP/NF and CoFe-LDH/CMP/NF. Lattice fringe spaces of 0.233 and 0.265 nm correspond to (112) crystallographic planes of CMP and (015) planes of CoFe-LDH/CMP have been barely found in the inverse FFT images (see Fig. 3-8c and Fig. 3-8f) [25].High-resolution TEM images (Fig. 3-8) imply the poor crystallinity structure of CMP/NF and CoFe-LDH/CMP/NF. Lattice fringe spaces of 0.233 and 0.265 nm correspond to (112) crystallographic planes of CMP and (015) planes of CoFe-LDH/CMP have been barely found in the inverse FFT images (see Fig. 3-8c and Fig. 3-8f) [25].

3.3. X-ray photoelectron and XRD diffractometry

Further analysis of the CoMoP electrocatalyst was performed using XPS to recognize the chemical states of the electrodes (see Figs. 3-10a-c) [48]. Figs. 3-11a-c show the XPS survey spectra for as-synthesized CMP, MoP, CoP, A-LDH/CMP, and A-LDH/NF confirm the presence of Mo, Co, P, Fe, and Ni in the samples. The case of Co 2p spectrum displays two distinct peaks which are ascribed to Co $2p_{3/2}$ and Co $2p_{1/2}$, components and the corresponding satellites peaks (identified as Sat.) are accompanied (Fig.3-9a, Fig.3-10a). Based on the literature reports, in the case of CMP on NF, Co^{2+} $2p_{3/2}$ peak at 779.2 eV is ascribed to the Co

oxidation state, which corresponds to Co-PO_x [25]. Meanwhile, the binding energies at 795, 798.4 eV can be assigned to Co-P, representing oxidized Co, while, in Co $2p_{3/2}$ region, the peak of Co^{3+} located at 783.5 eV is assigned to the Co-P [31]. In respect of the Co 2p spectra in bare CoP and CMP, the binding energy is down-shifted by ~0.2 eV. The introduction of Mo in the electronic structure of Co causes this down-shift [48]along with a strong electronic interaction between Mo and Co centers which facilitates the adsorption energy of H atoms [49] . The binding energy difference between the Co $2p_{3/2}$ and Co $2p_{1/2}$ peaks in all samples are

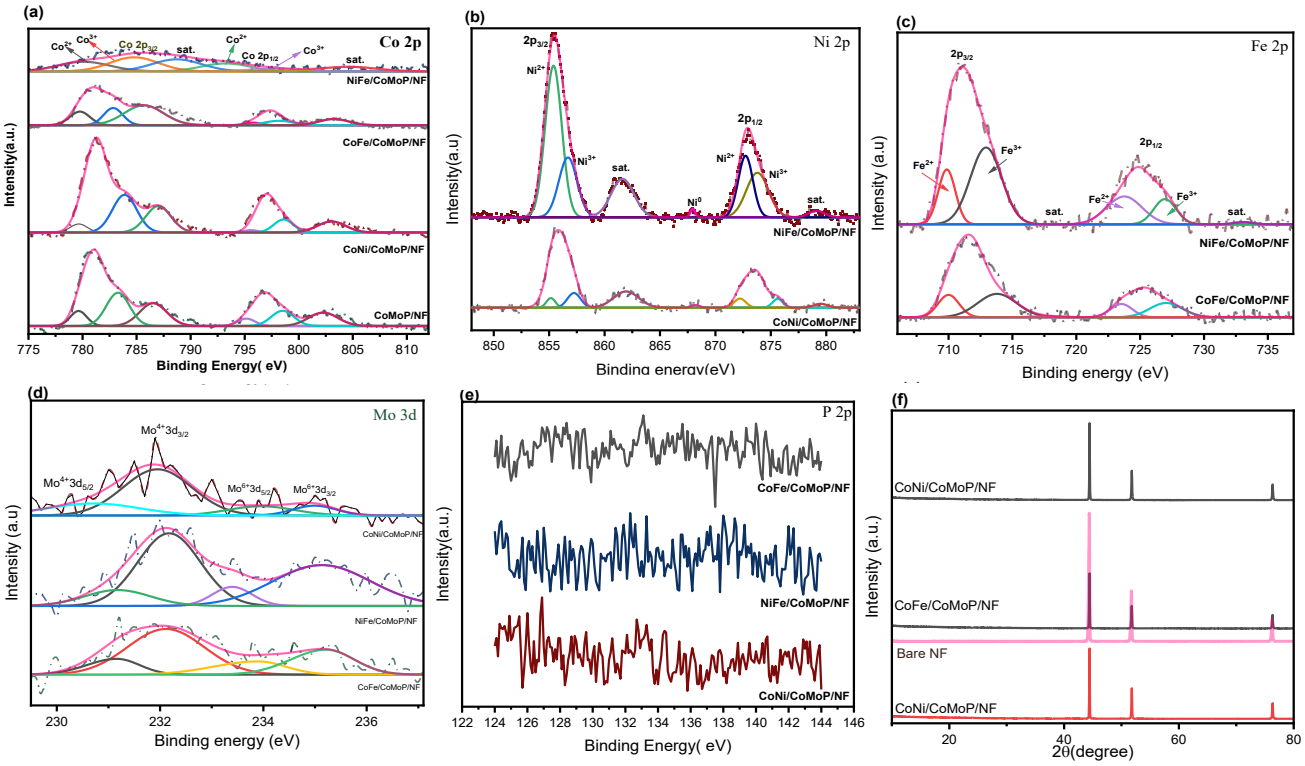

Fig. 3-9.XPS result of a) Co, b) Ni, C) Fe, d) Mo, e) P and f) XRD results of CoFe LDH, CoNi-LDH and NiFe-LDH on the CMP.

almost 16 eV, which is indicative of the Co^{2+} and Co^{3+} species (Fig.3-10a). In the full XPS spectra survey shown in Fig. 3-9a, Co 2p have the same Peaks even after A-LDH electrodeposition on NF with a positive shift of binding energies. This information implies a reduction in electron density around the Co sites in CoFe sample, as compared to those of CoNi-LDH/CMP and CMP [41]. Co 2p peaks in NiFe-LDH/CMP sample are not obvious as well as in other samples, which is partly due to the second electrodeposition and having lower cobalt content in comparison with other samples. Also, a high-resolution Co 2p XPS spectrum in Fig. 3-10d shows that Co with different valence states (Co^{2+} and Co^{3+}) exists on CoNi-LDH and CoFe-LDH. In addition, in both CoNi-LDH/NF and CoFe-LDH/NF, metallic Co have been

appeared at around 775.7 and 775 eV, respectively. However, the peak was not shown in other cobalt-contained samples, which could be due to the existence of precipitates away from the surface [50]. High resolution spectra of CoNi-LDH/NF (Fig.3-10d) show the presence of Co $2p_{3/2}$, Co $2p_{1/2}$, Co^{2+}, Co^{3+}, and satellite peaks at 781.2 eV, 796.7 eV, (783.8, 798 eV), (781.3, 796.2 eV), and (788.5, 802 eV), respectively[51]. The binding energies at (780.7, 798.8 eV), (783, 800 eV), (780.6, 796.5 eV), (787, 802.5 eV) ascribed to the three doublets of Co $2p_{3/2}$ and Co $2p_{1/2}$, Co^{2+} and Co^{3+}, satellite peaks in CoFe-LDH/NF[52]. Binding energy difference between Co $2p_{3/2}$ and Co $2p_{1/2}$ peaks in CoNi-LDH/NF is consistent with a Co^{2+} state[53]. Like CoFe-LDH/CMP/NF, CoFe individually electrodeposited on NF shows a positive shifting of binding energies, clearly indicating that CoNi/NF experiences more valence state around Co sites compared with CoFe-LDH/NF.

The P 2p region (Fig. 3-10b) displays a broad peak at 132.7 eV that can be assigned to surface oxidized P species in CMP, MoP and CoP. Their binding energies have the following order: CMP>MoP>CoP[54]. The change of binding energy in the mentioned samples illustrated that the charge redistribution happens as a result of strong electronic interaction between Mo and

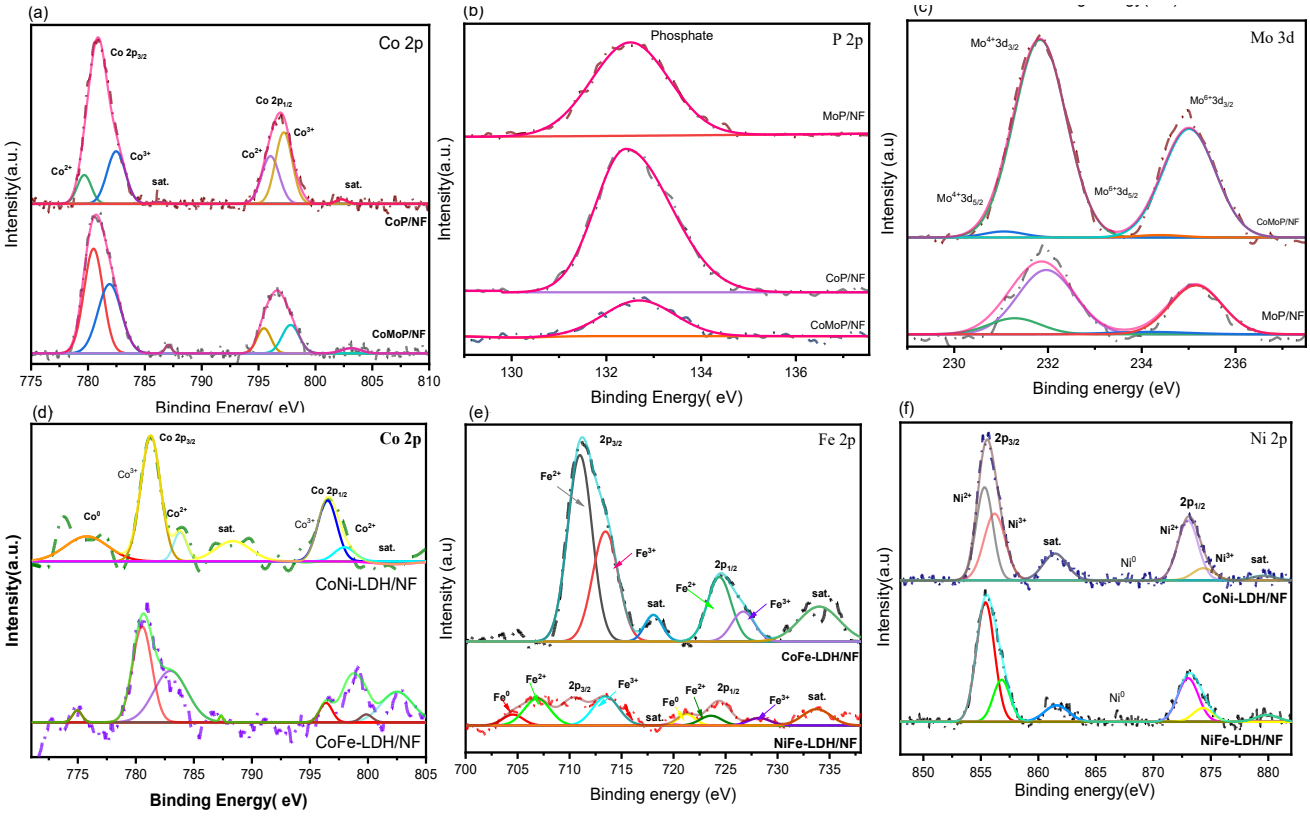

Fig. 3-10.Full-scan XPS spectra of CMP/NF, CoP/NF, MoP/NF (a) Co 2p ,(b) P 2p ,(c) Mo 3d and Full-scan XPS spectra of CoNi-LDH/NF, CoFe-LDH/NF and NiFe-LDH/NF d) Co 2p, e) Fe 2p , f) Ni 2p

Co centers, which could dramatically improve the electrocatalytic activity [34]. Based on the EDX elemental mapping analysis, P has been distributed in the CoMoP sample. Considering the different penetration depths of XPS and EDX, and a comparison of atomic ratio of P and Co in the XPS, it can be proposed that P was coated by Co in the outer layer; hence, the P, which was found by EDX, were not detected by XPS [55] . With that knowledge in mind, we can speculate that disappearing peak around 130 eV in XPS analysis for CoP and MoP samples has the same reason.

In the analysis of Mo 3d spectrum shown in Fig. 3-9d and Fig. 3-10c, two main peaks are indexed to Mo^{4+} 3d3/2 and Mo^{6+} 3d3/2 while the other two peaks suggest the presence of Mo^{4+} and Mo^{6+} in MoP and CMP (Fig. 3-10c) both of which are attributed to the surface oxidation of samples [41]. In addition, it should be mentioned that the binding energy of both Mo^{6+} 3d5/2 and Mo^{4+} 3d5/2 peaks of CoFe-LDH/CMP was slightly shifted to the right compared to CMP and CoNi (Fig. 3-9d).

The presence of Ni species in different states was observed in Ni 2p region spectrum (Fig. 3-9b). The pair peaks of Ni can be assigned to Ni^{2+} and Ni^{3+}, both together arising from the surface oxidation of phosphides. Meanwhile, Ni 2p3/2 peaks at 855.8 and 855.6 eV are

The Fe 2p core-level spectra were comprised of Fe $2p_{1/2}$ and Fe $2p_{3/2}$ spin-orbit peaks (Fig. 3-9c), which implies the oxidation state of Fe^{3+}(0d) [46]. Furthermore, the CoFe-LDH/CMP signal shows the peaks at 711.5 eV ($2p_{3/2}$) and 724.9 eV ($2p_{1/2}$) belonging to Fe^{2+}. Compared to the NiFe-LDH/CMP, Fe 2p peaks shifted positively by 0.4 eV suggest that Fe sites have increased valence state [58] and act as main active centers that facilitate the first step of HER (adsorption of H atoms) [49]. The Fe species in the CoFe-LDH/NF were deconvoluted into several peaks, which are dominated by the Fe $2p_{3/2}$ oxidation state (Fig. 3-10e). In this sample, the Fe2p spectrum contains Fe $2p_{3/2}$ (711.2 eV), Fe $2p_{1/2}$ (724.6 eV), Fe^{2+} (711,724.4 eV) and Fe^{3+} (713.4,726.6 eV), respectively. Peaks of Fe $2p_{1/2}$ and Fe $2p_{3/2}$ are consistent with the occurrence of $Fe(OH)_3$ units in CoFe-LDH [59]. NiFe-LDH electrodeposited on nickel foam solely have the all peaks of CoFe-LDH/NF plus Fe^0 (704.3, 721.2 eV), which discloses the zero-valence state of Fe, evidencing the metallic Fe in NiFe alloy[60].

The XRD patterns of electrodeposited LDH layers on CMP, shown in Fig. 3-9f and Fig. 3-11d, demonstrate their intensity variation between the species electrodeposited on NF and with bare NF. The intensity of diffracted peaks of all samples is lower, as compared to the bare Ni foam,

they are in a good agreement with EDS mapping results (see Figs. 3-4 to3-7), suggesting the presence of electrodeposited material. The XRD results show three main diffraction peaks obtained from the substrate (NF) due to the low thickness of the CMP and A-LDH/CMP electrodeposited on the nickel foam. These peaks (44.3, 51.5, and 76.1) match crystallographic planes ((111), (200), and (220)) of metallic nickel, respectively. However, no diffraction peaks were indicated, except for Ni, which may be due to very low crystallinity (amorphous structure) and a tiny amount of dissolved electrocatalyst [61].

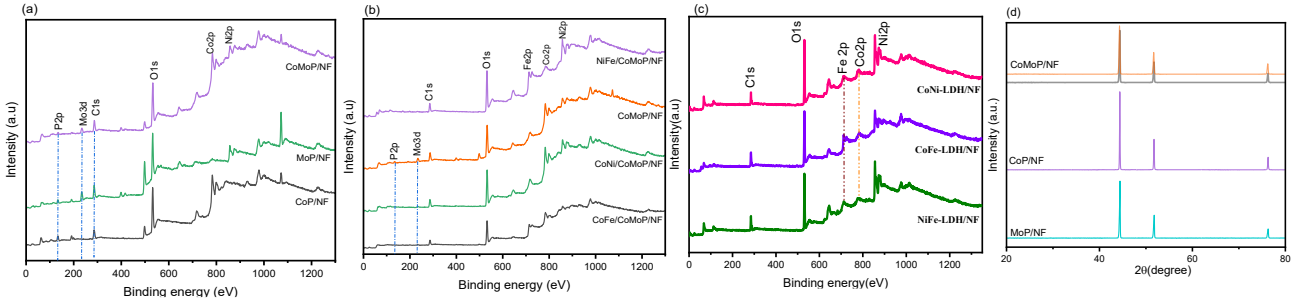

Fig. 3-11.a-c) survey spectra of different materials, d) XRD results of MoP/NF, CoP/NF and CMP/NF.

3.4. HER activity and stability

Polarization curves (Fig. 3-12a-b and Fig. 3-13a-b) showed that the CoFe-LDH had better activities than other materials, due to its high current response and small overpotential. As shown in Fig. 3-13b, to reach a current density of 10 $mA.cm^{-2}$, the required overpotential are 209, 447, and 447 mV for CMP/NF, CoP/NF, and MoP/NF, respectively. Tafel slope is considered to be one of the important factors that reflects the catalytic behavior and the reaction mechanism. Fig. 3-12c revealed that CMP has a lower Tafel slope (78.1 $mV.dec^{-1}$) than CoP (118 $mV.dec^{-1}$) and MoP (108 $mV.dec^{-1}$). Tafel slope in the range of 40–120 $mV \cdot dec^{-1}$ reveals that the HER on their surface is consistent with the Volmer-Heyrovsky mechanism [40]. The CMP under alkaline conditions has a superior HER catalytic activity as compared to other phosphides (Fig. 3-13a-b). This is because phosphorus had relatively a higher electronegativity than cobalt or molybdenum, so, they are positively charged, which lead to strong adsorption capacity for the HER intermediates [49]. Theoretical calculation results revealed that both Gibbs adsorption-free energies of OH^- and H_2O in cobalt phosphide are distinctly bigger than those of molybdenum-doped cobalt phosphide [49]. Fig. 3-12b indicates that the CoFe-LDH/CMP/NF required only an overpotential of 22.4 mV to reach a current response 30 $mA.cm^{-2}$, which is much smaller than NiFe-LDH/CMP/NF (383 mV), CoNi-LDH/CMP/NF

(117 mV) and CMP/NF (275.7) [39]. Additionally, CoFe-LDH/CMP/NF has a low Tafel slope of 64.3 mV.dec^{-1}, which is significantly lower than 79.3, 78.1 and 78 mV.dec^{-1} for NiFe-LDH/CMP, CMP and CoNi-LDH/CMP, respectively (Fig. 3-12c). Figs. 3-14b-c summarized

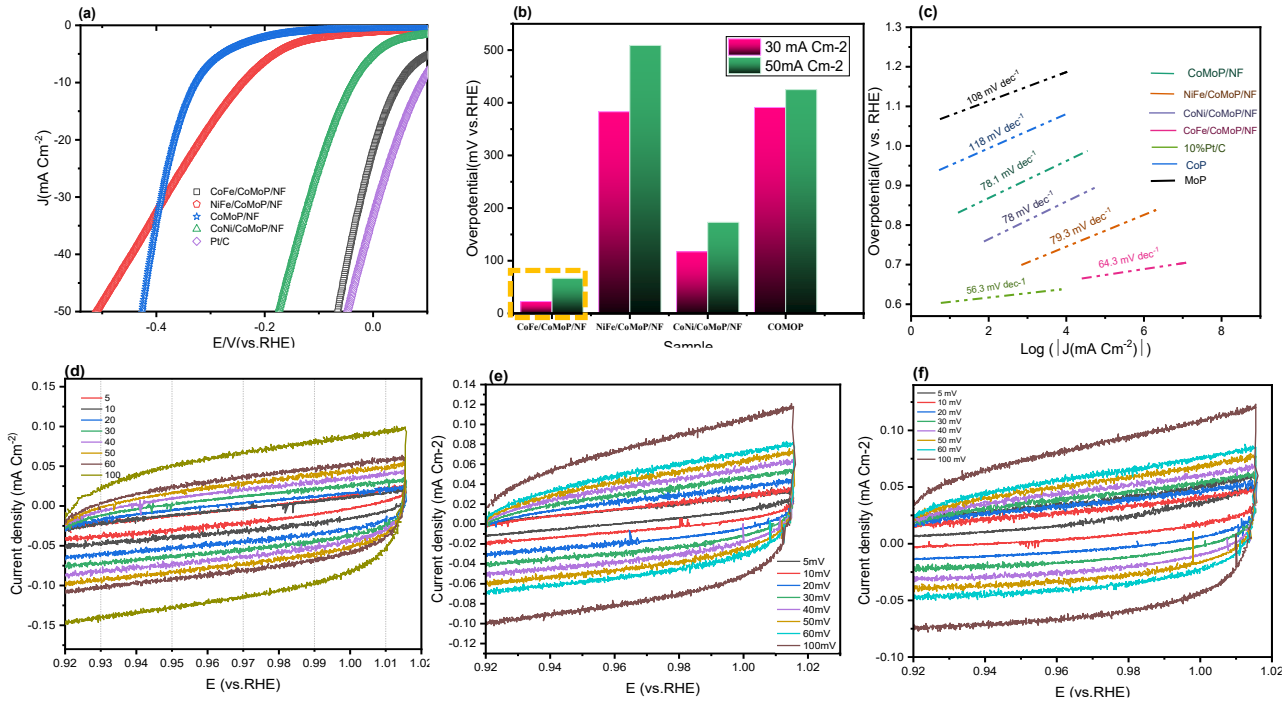

Fig. 3-12. a) LSV plots at 5 mV, (b) Overpotential at different current densities, (c) Tafel slopes of CoFe-LDH/CMP, CMP, Pt/C, NiFe- LDH and CoNi-LDH and CV plots of all scan rate of d) CoFe-LDH/CMP, e) CoNi-LDH/CMP and f) NiFe-LDH/CMP.

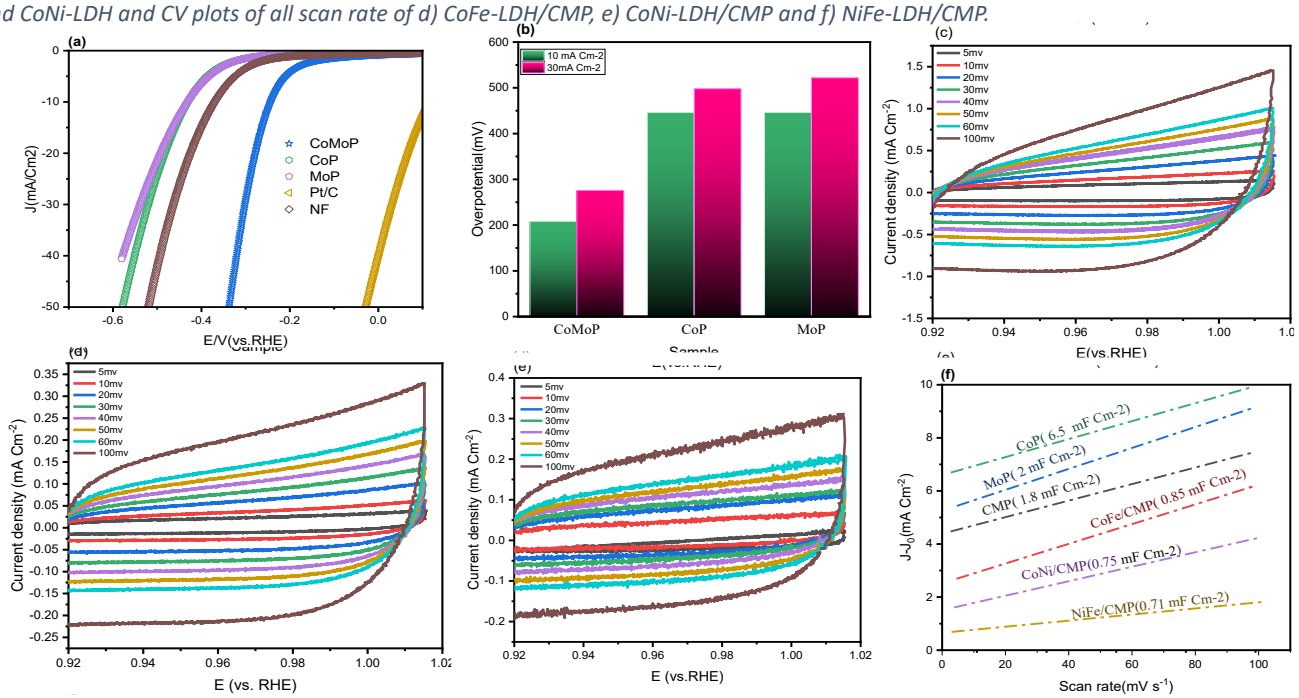

Fig. 3-13. (a) LSV plots at 5 mV of different samples, (b) Overpotential at different current densities and CV plots of all scan rates of C) CoP/NF, d) MoP/NF, e) CMP/NF and f) Cdl values of different materials.

the performance of CoP based and LDH-based electrocatalyst in recent literatures and compare it with this study. The low overpotential and Tafel slope of CoFe-LDH/CMP in comparison with other research, suggests the outstanding kinetics of HER reaction, which can be attributed to the synergistic effect of the CoFe-LDH and CoMoP [46]. It can be concluded that the Volmer-Heyrovsky mechanism is the rate control step of the HER for the A-LDH/CMP samples. Meanwhile, the Tafel slope of the CoFe-LDH/CMP has also been found to be considerably less than the CMP slope. This means that the second electrodeposition gives desorption of H* on the electrode surface, leading to improvement of the catalytic activity of the prepared electrode. The proposed mechanism of the electrocatalyst (CoFe-LDH/CMP/NF) is delineated in more detail (see Fig.3-15). Water molecules on the surface of CMP form an electrical double layer (EDL), where interactions occur among oxygen atoms, the sites coordinated metal (Co, Fe), weaken the H-OH bond. In other words, the H-OH bonds are weakened by electronic effects[59]. Second, free electrons cause the dissociation of H_2O molecules into H^+ and OH^-. In the end, hydrogen atoms are absorbed on the vacant metal sites next to the one covered by the OH^-, which is denoted as adsorbed H[62]. Therefore, the entire rise to the of OH^-, and the alkaline HER process depends on the kinetics of the recombination of adsorbed H atoms and the desorption of OH^- [46]. The electrochemical double- layer capacitance (Cdl) was measured

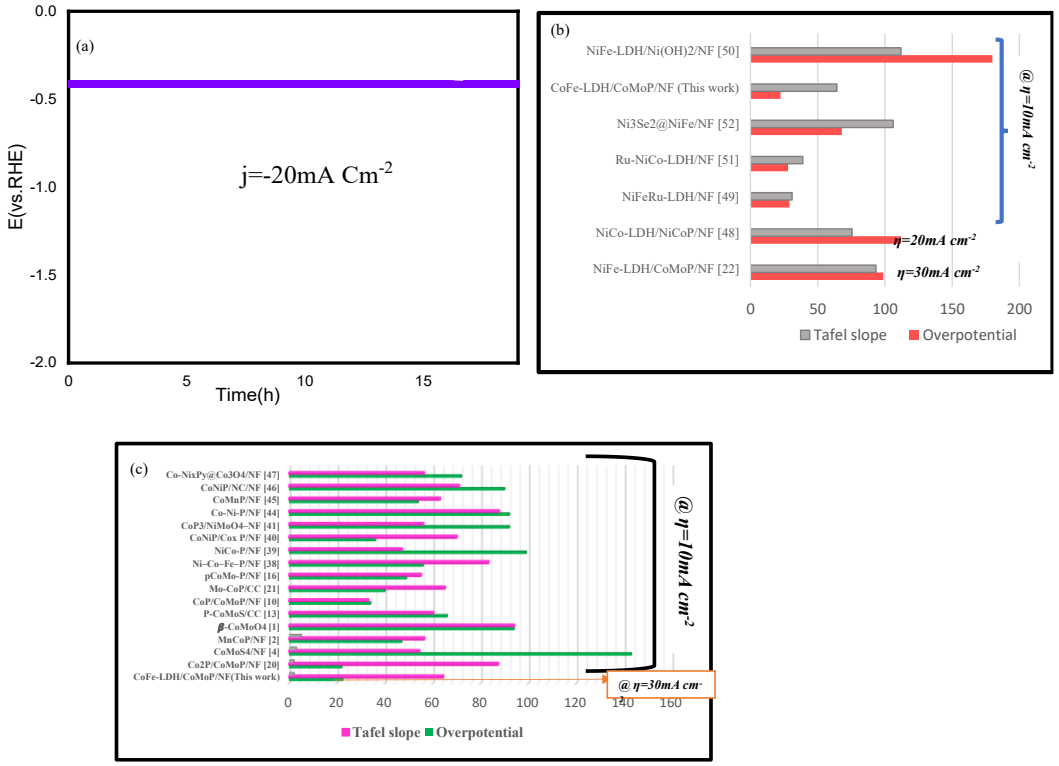

Fig. 3-14.a) stability test of CoFe-LDH/CMP/NF, Comparison between this work and previously reported b) LDH- based electrocatalyst and c) CoP-based electrocatalyst to previously reported catalysts.

through the CV test in the non-Faraday potential window at the aforementioned scan rates (Figs. 3-13c-e and Figs 3-12d-f). Fig. 3-13f is a fitting diagram of the △j (the difference in positive/negative scanning current density) as a function of scan rate at a potential window median of 0.97 V (vs. RHE). Based on the Fig. 3-13f, C_{dl} values of CMP, CoP, MoP, NiFe-LDH/CMP, CoFe-LDH/CMP and CoNi-LDH/CMP samples were 1.8, 6.5, 2, 0.71, 0.85 and 0.75 $mF.cm^{-2}$, respectively [63].

To better understand the dynamic of the HER process, properties of electrode materials, and electrode reactions, the electrochemical impedance spectroscopy (EIS) test was conducted (Figs. 3-16). The Randles circuit with just a simple semi-circle is most expected in the EIS analysis. Surprisingly, EIS results of prepared electrodes (Figs. 3-16) exhibit a combination of Warburg impedance (straight line) and charge transfer resistance (Randles circuit) . It can be observed that CoFe-LDH/CMP/NF and CMP/NF exhibit both smaller radius in the semi-circle (electrolyte resistance RS) compared to the LDH-based electrocatalyst and both CoP/NF and MoP/NF, suggesting their low charge transfer resistance [64].

Another way to investigate catalyst performance is through the stability test of the material done by CP. Stability test results (Fig. 3-14a) show no potential change for 19 hours at the current density of -20 $mA.cm^{-2}$, indicating that CoFe-LDH/CMP electrode has excellent stability in alkaline electrolytes.

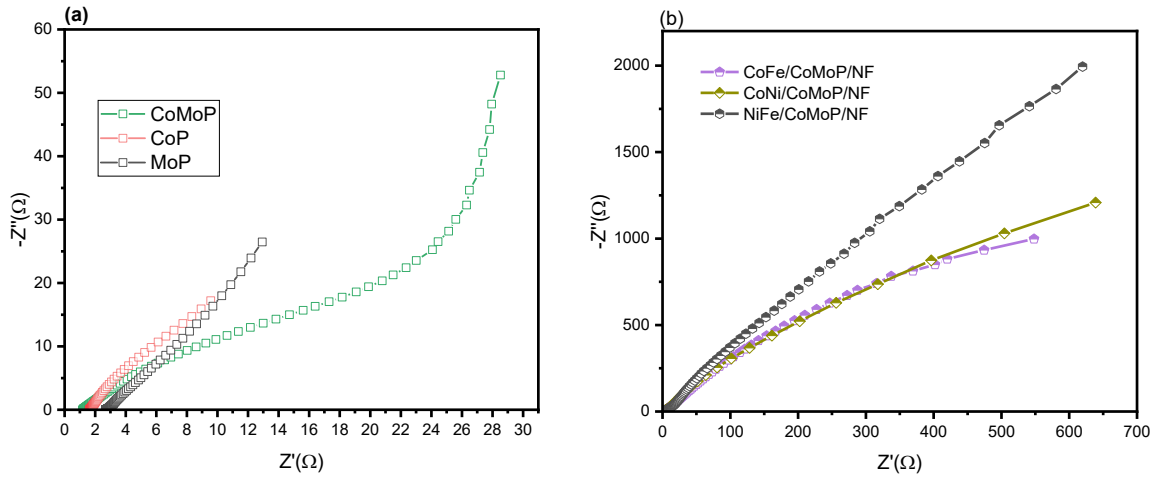

Fig. 3-15.EIS measurement of different material at a) first electrodeposition and b) second electrodeposition.

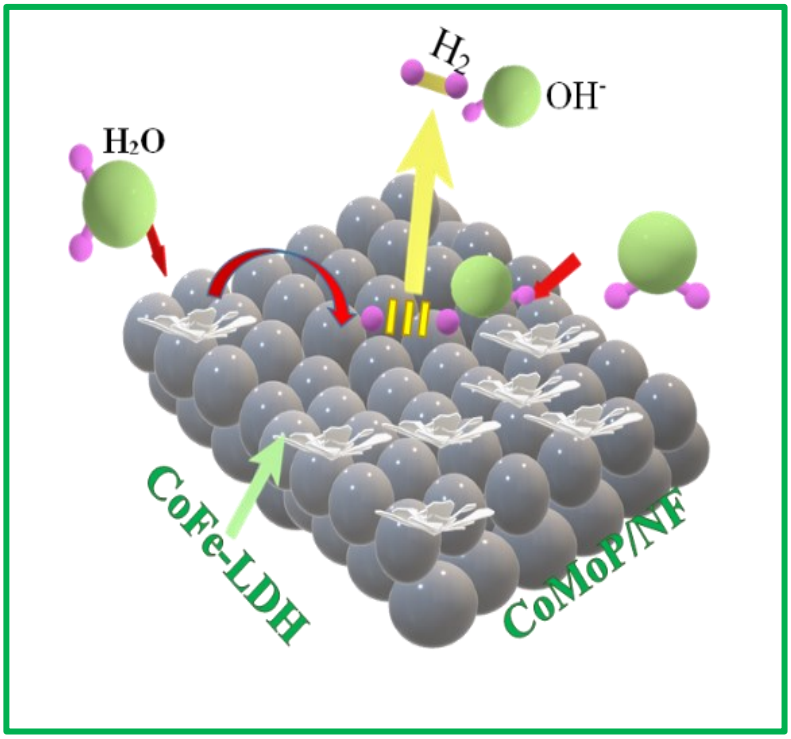

Fig. 3-16.Schematic representation of the HER process on the surface of the CoFe-LDH/CMP/NF

Chapter 4: Conclusion

In this study, transition metal phosphides (TMPs) were electrodeposited on the nickel foam and HER performance of A-LDHs electrodeposited on TMPs was investigated. TMPs (CMP/NF, CoP/NF, and MoP/NF) need 209, 447, and 447 mV overpotential, respectively, to reach a current density of 30 $mA.cm^{-2}$. CoFe-LDH/CMP showed the best performance by requiring an overpotential of 22.4 mV to reach a current response of 30 $mA.cm^{-2}$, while NiFe-LDH/CMP and CoNi-LDH/CMP needed 383 and 117 mV. The strong synergistic effects of the CoFe-LDH nanoflower and CMP, with the typical 3D interconnected architectures, optimize the binding energies of reaction intermediates and promote charge transfer between CoFe-LDH and CMP, ultimately enhancing the catalytic performance. This study offers an effective strategy for developing durable, earth-abundant transition metal-based electrocatalysts for enhanced HER. The present synthesis approach with optimum dopants can be used to develop cost-effective and high efficiency electrocatalysts that can act as an excellent replacement for non-noble metal HER electrocatalysts.

Chapter 5: Future work

Currently, single atom electrocatalysis (SAE) holds great promise for maximized metal utilization and exceptional tunability of the catalytic site. The issue with most single atom electrocatalyst is using high temperature in synthesizing it and stability of single atom[65]. In most of the reported cases, single metal atom species have been anchored by p-block elements, metal organic frameworks, and metal hydroxides. LDHs and their derivatives with long-time stability, low cost and easy synthesis are a good support for single noble atom[65]. Utilization of LDH as a support for SAE will be my next research. With the joint efforts of scientists from all over the world, I hope in future, LDH-based electrocatalyst will be used on an industrial scale for HER.

References

[1] A. Raihan, Nexus between greenhouse gas emissions and its determinants: The role of renewable energy and technological innovations towards green development in South Korea, Innovation and Green Development, 2 (2023) 100066.

[2] R.J.D.B.S.C. Holly Shaftel, What Is Climate Change? (n.d.).

[3] W.C. Jeong, D.H. Lee, J.H. Roh, J.B. Park, Scenario Analysis of the GHG Emissions in the Electricity Sector through 2030 in South Korea Considering Updated NDC†, Energies (Basel), 15 (2022).

[4] C. Ji, T. Hong, H. Kim, Statistical analysis of greenhouse gas emissions of South Korean residential buildings, Renewable and Sustainable Energy Reviews, 156 (2022).

[5] C.J. Fetrow, C. Carugati, X.D. Zhou, S. Wei, Electrochemistry of metal-CO2 batteries: Opportunities and challenges, Energy Storage Mater, 45 (2022) 911–933.

[6] M. Younas, S. Shafique, A. Hafeez, F. Javed, F. Rehman, An Overview of Hydrogen Production: Current Status, Potential, and Challenges, Fuel, 316 (2022).

[7] J.A. Okolie, B.R. Patra, A. Mukherjee, S. Nanda, A.K. Dalai, J.A. Kozinski, Futuristic applications of hydrogen in energy, biorefining, aerospace, pharmaceuticals and metallurgy, Int J Hydrogen Energy, 46 (2021) 8885–8905.

[8] N. Sazali, Emerging technologies by hydrogen: A review, Int J Hydrogen Energy, 45 (2020) 18753–18771.

[9] J. Chi, H. Yu, Water electrolysis based on renewable energy for hydrogen production, Cuihua Xuebao/Chinese Journal of Catalysis, 39 (2018) 390–394.

[10] L. Wan, Z. Xu, Q. Xu, M. Pang, D. Lin, J. Liu, B. Wang, Key components and design strategy of the membrane electrode assembly for alkaline water electrolysis, Energy Environ Sci, 16 (2023) 1384–1430.

[11] S. Shiva Kumar, H. Lim, An overview of water electrolysis technologies for green hydrogen production, Energy Reports, 8 (2022) 13793–13813.

[12] K. Zeng, D. Zhang, Recent progress in alkaline water electrolysis for hydrogen production and applications, Prog Energy Combust Sci, 36 (2010) 307–326.

[13] S. Hu, B. Guo, S. Ding, F. Yang, J. Dang, B. Liu, J. Gu, J. Ma, M. Ouyang, A comprehensive review of alkaline water electrolysis mathematical modeling, Appl Energy, 327 (2022).

[14] J. Brauns, T. Turek, Alkaline water electrolysis powered by renewable energy: A review, Processes, 8 (2020).

[15] D. Zhou, P. Li, W. Xu, S. Jawaid, J. Mohammed-Ibrahim, W. Liu, Y. Kuang, X. Sun, Recent Advances in Non-Precious Metal-Based Electrodes for Alkaline Water Electrolysis, ChemNanoMat, 6 (2020) 336–355.

[16] K. Wang, X. Wang, Z. Li, B. Yang, M. Ling, X. Gao, J. Lu, Q. Shi, L. Lei, G. Wu, Y. Hou, Designing 3d dual transition metal electrocatalysts for oxygen evolution reaction in alkaline electrolyte: Beyond oxides, Nano Energy, 77 (2020).

[17] M. Yang, Y. Jiang, M. Qu, Y. Qin, Y. Wang, W. Shen, R. He, W. Su, M. Li, Strong electronic couple engineering of transition metal phosphides-oxides heterostructures as multifunctional electrocatalyst for hydrogen production, Appl Catal B, 269 (2020).

[18] J. Xie, Y. Xie, Transition Metal Nitrides for Electrocatalytic Energy Conversion: Opportunities and Challenges, Chemistry - A European Journal, 22 (2016) 3588–3598.

[19] A.A. Yadav, Y.M. Hunge, S.W. Kang, Highly efficient porous morphology of cobalt molybdenum sulfide for overall water splitting reaction, Surfaces and Interfaces, 23 (2021).

[20] J. Theerthagiri, S.J. Lee, A.P. Murthy, J. Madhavan, M.Y. Choi, Fundamental aspects and recent advances in transition metal nitrides as electrocatalysts for hydrogen evolution reaction: A review, Curr Opin Solid State Mater Sci, 24 (2020).

[21] J. Su, J. Zhou, L. Wang, C. Liu, Y. Chen, Synthesis and application of transition metal phosphides as electrocatalyst for water splitting, Sci Bull (Beijing), 62 (2017) 633–644.

[22] A. Ali, F. Long, P.K. Shen, Innovative Strategies for Overall Water Splitting Using Nanostructured Transition Metal Electrocatalysts, Electrochemical Energy Reviews, 6 (2023).

[23] S. Dou, X. Wang, S. Wang, Rational Design of Transition Metal-Based Materials for Highly Efficient Electrocatalysis, Small Methods, 3 (2019).

[24] J. Peng, W. Dong, Z. Wang, Y. Meng, W. Liu, P. Song, Z. Liu, Recent advances in 2D transition metal compounds for electrocatalytic full water splitting in neutral media, Mater Today Adv, 8 (2020).

[25] W. Zhang, Y. Liu, H. Zhou, J. Li, S. Yao, H. Wang, A high-performance electrocatalyst of CoMoP@NF nanosheet arrays for hydrogen evolution in alkaline solution, J Mater Sci, 54 (2019) 11585–11595.

[26] C. Ray, S.C. Lee, K.V. Sankar, B. Jin, J. Lee, J.H. Park, S.C. Jun, Amorphous Phosphorus-Incorporated Cobalt Molybdenum Sulfide on Carbon Cloth: An Efficient and Stable Electrocatalyst for Enhanced Overall Water Splitting over Entire pH Values, ACS Appl Mater Interfaces, 9 (2017) 37739–37749.

[27] M. Zhai, F. Wang, H. Du, Transition-Metal Phosphide-Carbon Nanosheet Composites Derived from Two-Dimensional Metal-Organic Frameworks for Highly Efficient Electrocatalytic Water-Splitting, ACS Appl Mater Interfaces, 9 (2017) 40171–40179.

[28] L. Xiong, Y. Qiu, X. Peng, Z. Liu, P.K. Chu, Electronic structural engineering of transition metal-based electrocatalysts for the hydrogen evolution reaction, Nano Energy, 104 (2022).

[29] Z. Li, C. Zhang, Y. Yang, S. Pi, Y. Yu, C. Wan, B. Zhou, W. Chao, L. Lu, Molten-salt-induced phosphorus vacancy defect engineering of heterostructured cobalt phosphides for efficient overall water splitting, Inorg Chem Front, 10 (2022) 325–334.

[30] J. Chang, K. Li, Z. Wu, J. Ge, C. Liu, W. Xing, Sulfur-Doped Nickel Phosphide Nanoplates Arrays: A Monolithic Electrocatalyst for Efficient Hydrogen Evolution Reactions, ACS Appl Mater Interfaces, 10 (2018) 26303–26311.

[31] X. Chen, Q. Li, Q. Che, Y. Chen, X. Xu, Interface Engineering of Crystalline/Amorphous Co 2 P/CoMoP x Nanostructure as Efficient Electrocatalysts for Hydrogen Evolution Reaction, ACS Sustain Chem Eng, 7 (2019) 2437–2445.

[32] Z. Guo, L. Liu, J. Wang, Y. Cao, J. Tu, X. Zhang, L. Ding, Recent progress in CoP-based materials for electrochemical water splitting, Int J Hydrogen Energy, 46 (2021) 34194–34215.

[33] S.M. El-Refaei, S.M. El-Refaei, P.A. Russo, P. Amsalem, N. Koch, N. Pinna, The Importance of Ligand Selection on the Formation of Metal Phosphonate-Derived CoMoP and CoMoP2Nanoparticles for Catalytic Hydrogen Evolution, ACS Appl Nano Mater, 3 (2020) 4147–4156.

[34] X. Huang, X. Xu, X. Luan, D. Cheng, CoP nanowires coupled with CoMoP nanosheets as a highly efficient cooperative catalyst for hydrogen evolution reaction, Nano Energy, 68 (2020).

[35] L. Xu, Y. Sun, E. Wang, E. Shen, Z. Liu, C. Hu, Y. Xing, Y. Lin, H. Jia, A cobalt molybdenum phosphate with a

tunnel: Hydrothermal synthesis and structure of (NH 3 CH 2 CH 2 NH 3) 4 á (NH 3 CH 2 CH 2 NH 2) á Na á [Co 2 Mo 12 O 30 (PO 4)(HPO 4) 4 (H 2 PO 4) 3] á 5H 2 O, n.d.

[36] M. Zhu, J. Sun, Y. Cao, Y. Zhang, Z. Liu, X. Wang, Self-Supporting Honeycomb Nickel Cobalt Phosphide on Nickel Foam as an Efficient Electrocatalyst for the Hydrogen Evolution Reaction, Energy and Fuels, 36 (2022) 4895–4901.

[37] N. Iqbal, I. Khan, A. Ali, A. Qurashi, A sustainable molybdenum oxysulphide-cobalt phosphate photocatalyst for effectual solar-driven water splitting, J Adv Res, 36 (2022) 15–26.

[38] Y. Han, P. Li, Z. Tian, C. Zhang, Y. Ye, X. Zhu, C. Liang, Molybdenum-Doped Porous Cobalt Phosphide Nanosheets for Efficient Alkaline Hydrogen Evolution, ACS Appl Energy Mater, 2 (2019) 6302–6310.

[39] V.H. Hoa, D.T. Tran, D.C. Nguyen, D.H. Kim, N.H. Kim, J.H. Lee, Molybdenum and Phosphorous Dual Doping in Cobalt Monolayer Interfacial Assembled Cobalt Nanowires for Efficient Overall Water Splitting, Adv Funct Mater, 30 (2020).

[40] M. Shamloofard, S. Shahrokhian, Dual-electrocatalysis behavior of star-like zinc–cobalt-sulfide decorated with cobalt–molybdenum-phosphide in hydrogen and oxygen evolution reactions, Nanoscale, 13 (2021) 17576–17591.

[41] X. Liu, B. Wei, R. Su, C. Zhao, D. Dai, X. Ma, L. Xu, Mo-Doped Cobalt Phosphide Nanosheets for Efficient Hydrogen Generation in an Alkaline Media, Energy Technology, 7 (2019).

[42] S. Zhao, J. Berry-Gair, W. Li, G. Guan, M. Yang, J. Li, F. Lai, F. Corà, K. Holt, D.J.L. Brett, G. He, I.P. Parkin, The Role of Phosphate Group in Doped Cobalt Molybdate: Improved Electrocatalytic Hydrogen Evolution Performance, Advanced Science, 7 (2020).

[43] G.R. Williams, D. O'Hare, Towards understanding, control and application of layered double hydroxide chemistry, J Mater Chem, 16 (2006) 3065–3074.

[44] Q. Wang, D. Ohare, Recent advances in the synthesis and application of layered double hydroxide (LDH) nanosheets, Chem Rev, 112 (2012) 4124–4155.

[45] Z. Gu, J.J. Atherton, Z.P. Xu, Hierarchical layered double hydroxide nanocomposites: Structure, synthesis and applications, Chemical Communications, 51 (2015) 3024–3036.

[46] R. Yang, Y. Zhou, Y. Xing, D. Li, D. Jiang, M. Chen, W. Shi, S. Yuan, Synergistic coupling of CoFe-LDH arrays with NiFe-LDH nanosheet for highly efficient overall water splitting in alkaline media, Appl Catal B, 253 (2019) 131–139.

[47] Y. Wang, D. Yan, S. El Hankari, Y. Zou, S. Wang, Recent Progress on Layered Double Hydroxides and Their Derivatives for Electrocatalytic Water Splitting, Advanced Science, 5 (2018).

[48] H. Wu, W. Xiao, C. Guan, X. Liu, W. Zang, H. Zhang, J. Ding, Y.P. Feng, S.J. Pennycook, J. Wang, Hollow Mo-doped CoP nanoarrays for efficient overall water splitting, Nano Energy, 48 (2018) 73–80.

[49] W. Mai, Q. Cui, Z. Zhang, K. Zhang, G. Li, L. Tian, W. Hu, CoMoP/NiFe-Layered Double-Hydroxide Hierarchical Nanosheet Arrays Standing on Ni Foam for Efficient Overall Water Splitting, ACS Appl Energy Mater, 3 (2020) 8075–8085.

[50] C.C. Wang, M. Liu, B.Y. Man, C.S. Chen, S.Z. Jiang, S.Y. Yang, X.G. Gao, S.C. Xu, B. Hu, Z.C. Sun, J.J. Guo, J. Hou, Role of cobalt in room-temperature ferromagnetic Co-doped ZnO thin films, AIP Adv, 2 (2012).

[51] Z.Y. Tian, P.M. Kouotou, A. el Kasmi, P.H.T. Ngamou, K. Kohse-Höinghaus, H. Vieker, A. Beyer, A. Gölzhäuser, Low-temperature deep oxidation of olefins and DME over cobalt ferrite, Proceedings of the Combustion Institute,

35 (2015) 2207–2214.

[52] L. Jinlong, L. Tongxiang, Y. Meng, K. Suzuki, H. Miura, Comparing different microstructures of CoS formed on bare Ni foam and Ni foam coated graphene and their supercapacitors performance, Colloids Surf A Physicochem Eng Asp, 529 (2017) 57–63.

[53] X. Dai, Y. Dai, J. Lu, L. Pu, W. Wang, J. Jin, F. Ma, N. Tie, Cobalt oxide nanocomposites modified by NiCo-layered double hydroxide nanosheets as advanced electrodes for supercapacitors, Ionics (Kiel), 26 (2020) 2501–2511.

[54] T. Ahamad, M. Naushad, S.M. Alshehri, Fabrication of CoP based nanocomposite as an electrocatalyst for oxygen- and hydrogen-evolving energy conversion reactions, Mater Lett, 278 (2020).

[55] Z. Wu, Q. Gan, X. Li, Y. Zhong, H. Wang, Elucidating Surface Restructuring-Induced Catalytic Reactivity of Cobalt Phosphide Nanoparticles under Electrochemical Conditions, Journal of Physical Chemistry C, 122 (2018) 2848–2853.

[56] M. Yu, G. Moon, E. Bill, H. Tüysüz, Optimizing Ni-Fe Oxide Electrocatalysts for Oxygen Evolution Reaction by Using Hard Templating as a Toolbox, ACS Appl Energy Mater, 2 (2019) 1199–1209.

[57] J. Qu, F. Li, M. Wang, S. Subakti, M. Deconinck, G. Chen, Y. Li, L. Liu, X. Wang, M. Yu, D. Wolf, A. Lubk, B. Büchner, Y. Vaynzof, O.G. Schmidt, F. Zhu, One-Pot Synthesis of Nitrate-Intercalated NiFe Layered Double Hydroxides with an 82 Å Interlayer Spacing, Adv Mater Interfaces, 9 (2022).

[58] F. Nie, Z. Li, X. Dai, X. Yin, Y. Gan, Z. Yang, B. Wu, Z. Ren, Y. Cao, W. Song, Interfacial electronic modulation on heterostructured NiSe@CoFe LDH nanoarrays for enhancing oxygen evolution reaction and water splitting by facilitating the deprotonation of OH to O, Chemical Engineering Journal, 431 (2022).

[59] M. Arif, G. Yasin, M. Shakeel, M.A. Mushtaq, W. Ye, X. Fang, S. Ji, D. Yan, Hierarchical CoFe-layered double hydroxide and g-C 3 N 4 heterostructures with enhanced bifunctional photo/electrocatalytic activity towards overall water splitting, Mater Chem Front, 3 (2019) 520–531.

[60] Q. Shi, Q. Liu, Y. Ma, Z. Fang, Z. Liang, G. Shao, B. Tang, W. Yang, L. Qin, X. Fang, High-Performance Trifunctional Electrocatalysts Based on FeCo/Co2P Hybrid Nanoparticles for Zinc–Air Battery and Self-Powered Overall Water Splitting, Adv Energy Mater, 10 (2020).

[61] J. Lian, Y. Wu, J. Sun, High current density electrodeposition of NiFe/Nickel Foam as a bifunctional electrocatalyst for overall water splitting in alkaline electrolyte, J Mater Sci, 55 (2020) 15140–15151.

[62] N. Mahmood, Y. Yao, J.W. Zhang, L. Pan, X. Zhang, J.J. Zou, Electrocatalysts for Hydrogen Evolution in Alkaline Electrolytes: Mechanisms, Challenges, and Prospective Solutions, Advanced Science, 5 (2018).

[63] Y. Lin, M. Liu, Y. Pan, J. Zhang, Porous Co–Mo phosphide nanotubes: an efficient electrocatalyst for hydrogen evolution, J Mater Sci, 52 (2017) 10406–10417.

[64] M. Xiao, Y. Miao, Y. Tian, Y. Yan, Synthesizing nanoparticles of Co-P-Se compounds as electrocatalysts for the hydrogen evolution reaction, Electrochim Acta, 165 (2015) 206–210.

[65] Z. Zhang, P. Li, X. Zhang, C. Hu, Y. Li, B. Yu, N. Zeng, C. Lv, J. Song, M. Li, Recent advances in layered-double-hydroxides based noble metal nanoparticles efficient electrocatalysts, Nanomaterials, 11 (2021).

Publication and Conferences

List of conferences

[1] Y. Shajirati, M.M. Momeni, M. Tayebi, B.-K. Lee, 9th International Conference on Sustainable Solid Waste Management (CORFU2022), June 15-18, 2022, Greece (poster presentation)
[2] Y. Shajirati, M.M. Momeni, M. Tayebi, B.-K. Lee, 7th international conference on advance in functional materials (AFM2023), January 9-12, 202, Japan (poster presentation)
[3] Y. Shajirati, M. Razavi, B.-K. Lee, KOSAE 65th Annual Conference 2022 Proceedings, Oct. 26-28 ,2022, South Korea(Oral presentation)

List of publication

[1] Y. Shajirati, M.M. Momeni, M. Tayebi, B.-K. Lee, Facile synthesis of interlaced flower-like layered double hydroxides grown on porous CoMoP as a highly efficient electrocatalyst for hydrogen evolution reaction, Energy, 278 (2023), Article 127840

Energy 278 (2023) 127840

Contents lists available at ScienceDirect

Energy

journal homepage: www.elsevier.com/locate/energy

Facile synthesis of interlaced flower-like layered double hydroxides grown on porous CoMoP as a highly efficient electrocatalyst for hydrogen evolution reaction

Yasamin Shajirati [a], Mohamad Mohsen Momeni [b], Meysam Tayebi [c], Byeong-Kyu Lee [a,*]

[a] Department of Civil and Environment Engineering, University of Ulsan, Daehakro 93, Namgu, Ulsan 44610, Republic of Korea
[b] Department of Chemistry, Isfahan University of Technology, Isfahan 84156-83111, Iran
[c] Advanced Industrial Chemistry Research Center, Advanced Convergent Chemistry Division, Korea Research, Institute of Chemical Technology (KRICT), 45 Jonggaro, Ulsan 44412, Republic of Korea